

## ABSTRACT

CALDERON, VICTOR ALEJANDRO. Condition Dependent Performance Based Design. (Under the direction of Dr. Mervyn Kowalsky.)

Structures located in seismic regions are often subjected to multiple earthquakes. Multiple earthquakes can accumulate damage resulting in a deterioration of the seismic performance of a structure. In addition, aging of the structure can lead to corrosion that further propagates the deterioration. Past research has shown that the Park and Ang damage index (DI)(a demand parameter that quantifies damage) increases as damage aging conditions in the structures worsen or multiple seismic events are included in the analysis. This increases the probability of structures to collapse. This research proposes to study the effects of multiple earthquakes and damage accumulation in RC structures by developing strain based fragility functions for different aging conditions. To achieve this it is also important to develop limit states that represent corroded reinforcing steel. Therefore, a method to perform accelerated corrosion in passivated reinforcing steel rebars is proposed. These corroded rebars are then subjected to tension tests and buckled bar tension tests, which will be used to define service and damage control limit states. To show the relevance of this study a framework that incorporates corrosion models into a nonlinear time history analysis (NLTHA) is developed. A series of SDOF cantilever columns are subjected to a sweep of earthquakes. Preliminary results show that there is an increase in the probability of reaching a limit state when corrosion level increases. The results also show large dispersion of results when using PGA as the intensity measure (IM), indicating the need for a better intensity measure. The results of this research will (1) develop fragility curves that consider strain limit states to measure damage while incorporating different aging conditions, (2) establish limit states for corroded rebars, (3) inform the research community on the necessary methodology to accurately model corrosion for material testing and large scale testing of corroded reinforced members (4) consider the effects of multiple earthquakes with mainshock-aftershock sequences (5) incorporate the results into the direct displacement-based design methodology.

© Copyright 2020 by Victor Alejandro Calderon

All Rights Reserved

Condition Dependent Performance Based Design

by  
Victor Alejandro Calderon

A research proposal submitted to the Graduate Faculty of  
North Carolina State University  
in partial fulfillment of the  
requirements for the Degree of  
Doctor of Philosophy

Civil Construction and Environmental Engineering

Raleigh, North Carolina

2020

APPROVED BY:

---

Dr. James Nau

---

Dr. Mohammad Pour-Ghaz

---

Dr. Rudolf Seracino

---

Dr. Thomas Birkland

---

Dr. Mervyn Kowalsky  
Chair of Advisory Committee

## TABLE OF CONTENTS

<b>LIST OF TABLES . . . . .</b>	<b>iv</b>
<b>LIST OF FIGURES . . . . .</b>	<b>v</b>
<b>Chapter 1 Introduction . . . . .</b>	<b>1</b>
1.1 Scope and layout . . . . .	3
<b>Chapter 2 Literature review . . . . .</b>	<b>4</b>
2.1 Corrosion . . . . .	4
2.1.1 Time to corrosion . . . . .	5
2.1.2 Rate of corrosion . . . . .	6
2.1.3 Corrosion modified properties of reinforcing steel bars . . . . .	8
2.1.4 Physical test on corroded RC Structures . . . . .	9
2.2 Steel strain aging . . . . .	11
2.2.1 Metallurgical process . . . . .	11
2.2.2 Strain aging effects in structures . . . . .	12
2.3 Damage Indexes . . . . .	13
2.4 Multiple earthquake loading . . . . .	16
2.4.1 Mainshock-aftershock sequences loading . . . . .	16
2.4.2 Mainshock sequences loading . . . . .	18
2.5 Aging of structures . . . . .	20
2.6 Research Gap . . . . .	22
2.6.1 Objectives . . . . .	23
<b>Chapter 3 Experimental phase: mechanical properties and performance of corroded reinforcing steel . . . . .</b>	<b>24</b>
3.1 Proposed experimental campaign . . . . .	24
3.2 Expected outcomes from experimental phase . . . . .	32
<b>Chapter 4 Methodology . . . . .</b>	<b>33</b>
4.1 Modeling of corrosion for structural analysis . . . . .	33
4.2 Modeling of strain aging for structural analysis . . . . .	34
4.3 Multiple seismic events . . . . .	34
4.3.1 Earthquake selection . . . . .	35
4.3.2 Discrete modeling of main shock series . . . . .	36
4.3.3 Multiple main shock series . . . . .	37
4.4 Analytical Model . . . . .	37
4.4.1 Cantilever column . . . . .	37
4.4.2 Strain penetration . . . . .	38
4.4.3 Design limit states . . . . .	41
4.5 Comparison with existing physical tests . . . . .	42
4.5.1 Pristine condition columns . . . . .	42
4.5.2 Accelerated corrosion columns . . . . .	42

4.6	Analytical framework . . . . .	45
4.7	Results from NLTHA . . . . .	46
4.7.1	Effect on structure response . . . . .	46
4.7.2	Development of cumulative distribution functions . . . . .	48
4.7.3	Results discussion . . . . .	49
4.8	Future topics . . . . .	49
<b>Chapter 5 Expected findings and schedule of work . . . . .</b>		<b>51</b>
<b>BIBLIOGRAPHY . . . . .</b>		<b>52</b>

## LIST OF TABLES

Table 2.1	Damage index level classification [60]	14
Table 3.1	Accelerated corrosion times in 3/4" rebar	27
Table 3.2	Corroded Rebar Test Matrix	31
Table 4.1	Design limit states	41
Table 4.2	Analysis matrix	46

## LIST OF FIGURES

Figure 2.1	Corrosion process in reinforcing steel bar [36] . . . . .	5
Figure 2.2	Concrete water to cement ratio vs rate of corrosion . . . . .	7
Figure 2.3	Diameter decrease due to corrosion . . . . .	7
Figure 2.4	Corrosion level vs time (years) . . . . .	8
Figure 2.5	Force displacement response of RC corroded columns [35] . . . . .	9
Figure 2.6	Corrosion process for RC column [35] . . . . .	10
Figure 2.7	Corroded rebars stress-strain curves [35] . . . . .	10
Figure 2.8	Strain aging effect on yield strength vs time (days) . . . . .	13
Figure 2.9	Park and Ang conceptual scheme . . . . .	14
Figure 2.10	Mainshock-aftershock sequence train of ground motions [44] . . . . .	18
Figure 2.11	Mainshock-aftershock sequence selection at T=0.4s for crustal earthquakes in Vancouver, British Columbia [52] . . . . .	19
Figure 2.12	Mainshock sequence selection at Eureka, CA [51] . . . . .	20
Figure 3.1	Rebars Passivation Process in Calcium Hydroxyde Pore Solution . . . . .	26
Figure 3.2	Rebar Specimen Geometry . . . . .	26
Figure 3.3	Rebars Ends Protection . . . . .	26
Figure 3.4	Accelerated corrosion process . . . . .	27
Figure 3.5	BBT Test sequence[5] . . . . .	28
Figure 3.6	a) Picture of buckled bar; (b) Position of optical markers and adjustment to neutral axis; (c) Calculation of curvature [4] . . . . .	30
Figure 3.7	(a) Ductile rebar fracture; (b) Brittle rebar fracture [4] . . . . .	30
Figure 3.8	BBT results for rebars with and without ribs [4] . . . . .	31
Figure 4.1	Corrosion modeling for structural analysis . . . . .	34
Figure 4.2	Mainshock selection from PEER NGA West2 database . . . . .	36
Figure 4.3	Structural Model a) SDOF Column b) Structural Model . . . . .	39
Figure 4.4	End point plastic hinge method [47] . . . . .	39
Figure 4.5	Section of the RC Column . . . . .	40
Figure 4.6	Force-Displacement results from experimental results [21] and analytical model . . . . .	43
Figure 4.7	Force-Displacement results from experimental RC column with corrosion in longitudinal bar (CL=9.5%) results [29] and analytical model (shown in lightblue) . . . . .	44
Figure 4.8	Strain hysteresis from experimental RC column with corrosion in longitudinal bar (CL=9.5%) results from analytical model . . . . .	45
Figure 4.9	Force-Displacement results . . . . .	47
Figure 4.10	Stress strain response for extreme rebar location . . . . .	47
Figure 4.11	CDF of steel yielding limit state using $IM = PGA$ . . . . .	48
Figure 4.12	CDF of steel yielding limit state using $IM = Sd(T_1)$ . . . . .	49

# Chapter 1

## Introduction

Structures are designed assuming their original condition remains intact through their service life. However, as structures age, they suffer various forms of degradation. In addition, they may be subjected to multiple discrete seismic events. Both of these items may impact structural performance. Consider an RC column and the limit state corresponding to bar buckling. The limit state displacement ( $\Delta$ ) to achieve bar buckling for a pristine column is different from a column subjected to corrosion. Similarly, multiple small seismic events may predispose the column to suffer longitudinal bar buckling for a lower level of seismic intensity. It is the goal of this research to incorporate both of these effects into the definition of performance limit states. This can potentially serve two purposes: a) for existing structures, assessment can consider likely current conditions, and b) for new structures, changes could be proposed to the initial design that could mitigate the effect of future condition degradation.

Structures subjected to multiple events and aging conditions should be considered in Performance-Based Earthquake Engineering (PBEE). Recent earthquakes sequences such as the Christchurch 2010, Umbria-Marche Earthquake 1997 and more recently the Puerto Rico Earthquakes 2020, have shown that structures after sustaining damage during a mainshock have then collapsed or sustained increased damage after being subjected to a large magnitude aftershock[1][7][37]. Researchers have used the Park and Ang damage index (DI) to quantify damage, which is expressed as a two-term expression. The first term relates to the maximum displacement and the second term relates to the inelastic energy dissipation [60]. The second term is associated with the inelastic cyclic behavior of structural components. In addition, the calibration factor is very small and contributes little to the damage index. If the damage index renders the inelastic cyclic behavior as negligible, it cannot accurately represent damage. Further, this damage index uses calibrated data to determine the strength degradation parameter that has a degree of

arbitrariness, which is undesirable [57]. In addition to the Park and Ang damage index, other measures of damage such as drift ratio based limit states have been incorporated into the PEER Performance-Based Design Probabilistic Framework[42][19][49]. The majority of these studies show that there is an increase in the probability of damage or even collapse of a structure due to repeated loading or aging conditions, such as high corrosion levels (CL). However, these results are based on the limitations presented by these damage measures [49]. A more deterministic approach to measure damage is to use strain limits as indicators of damage for RC bridge columns, where concrete compressive and reinforcing steel tensile strain limits are used as the damage measure [20]. These strain limits have been correlated to observed damage in large scale column tests. Therefore, we believe that our research will provide a realistic measure of the increase in damage for different limit states due to aging conditions and multiple earthquake loadings.

In addition, structures can have an existing condition such as corrosion that further deteriorates the performance of the structure. Corrosion is one of the aging conditions that more significantly deteriorates the seismic response of a structure. Thus, it is important to determine the limit states of corroded reinforcing steel. Currently, the literature has developed expressions that correlate the level of corrosion to the decrease in strength of the reinforcing steel[61][11]. However, these studies have utilized an accelerated corrosion process that does not consider the protective film that is developed on the reinforcing steel surface when it is embedded in concrete, a process known as passivation of the reinforcing steel [36][16]. For corrosion to occur, the protective film on the reinforcing steel bar must occur, this process is known as depassivation. Depassivation of the reinforcing steel greatly affects the behavior of reinforcing steel and can significantly modify the measured properties of the corroded reinforcing steel. Furthermore, no study has presented performance limit states on corroded reinforcement. Therefore, this research aims to close this gap by performing an experimental campaign. This experimental campaign consists of a series of tension tests and buckled bar tension tests to help define the performance limit states of corroded reinforcement. These results will then inform the computational model.

Moreover, there is a high likelihood for a structure in a high seismic region to be subjected to mainshock-aftershock sequence during its service life. Therefore, it is important to consider the effects of mainshock-aftershock sequences. A series of condition-dependent nonlinear time history analyses are performed on a cantilever RC bridge column. The analysis applies a series of MS-AS sequence for different ages of the structure. The material properties of the structure are changed as a function of the aging conditions (e.g. corrosion). At the end of each analysis, the main variables of the study are the limit state that was reached, the controlling mode of response (flexural or shear controlled), the equivalent viscous damping, and the accumulated deformations.

In summary, this research aims to consider the likely future condition (considering deterioration mechanism and multiple earthquake loadings) of a structure in defining strain-based performance limit states.

## 1.1 Scope and layout

This research proposal describes the main components and objectives for the graduate studies of the author of this document. Chapter 2 contains the literature review which summarizes the state of the art in damage measurements and performance-based design framework. Chapter 3 covers the experimental campaign in corroded reinforcing steel. Chapter 4 summarizes the experimental and analytical procedures relevant to this study. Chapter 5 details the processing of current results.

# **Chapter 2**

## **Literature review**

Bridges are designed based on discrete events assuming that the initial material and structure properties remain constant through the life of the bridge. The purpose of the research described is to study condition dependent performance based design that considers the material and geometric properties as the structure ages, and the effects of multiple and discrete events on the achievement of prescribed limit states.

In this chapter, the current knowledge of aging of structures, damage indexes, corrosion and multiple earthquake loading is presented. Then the study gap and the objectives of this research are defined.

### **2.1 Corrosion**

Corrosion is one of the main aging effects in RC structures. In RC structures after the concrete is cast a protective layer forms on the surface of the reinforcing steel, this process is known as passivation of the reinforcing steel. However, under conditions such as chloride attack the protective film can be broken, this process is known as depassivation. The depassivation process onset corrosion. Corrosion reduces the area of steel, and also modify the strength of the reinforcing steel. If corrosion degrades the structural performance of the reinforcing steel it will certainly degrade the overall strength of the system. The incidence of corrosion in RC structures in earthquake prone areas is that it could trigger unintended seismic performance on a structure that was designed for pristine conditions. Therefore it is important to incorporate the mechanics of corrosion in this condition dependent performance based seismic design. The general chloride attack corrosion process can be explained using three main parameters such as (1) time to initiation of corrosion, (2) corrosion growth in reinforcing steel, and (3) the mechanical

properties of corroded reinforcing steel. Figure 2.1 schematically shows the corrosion process.

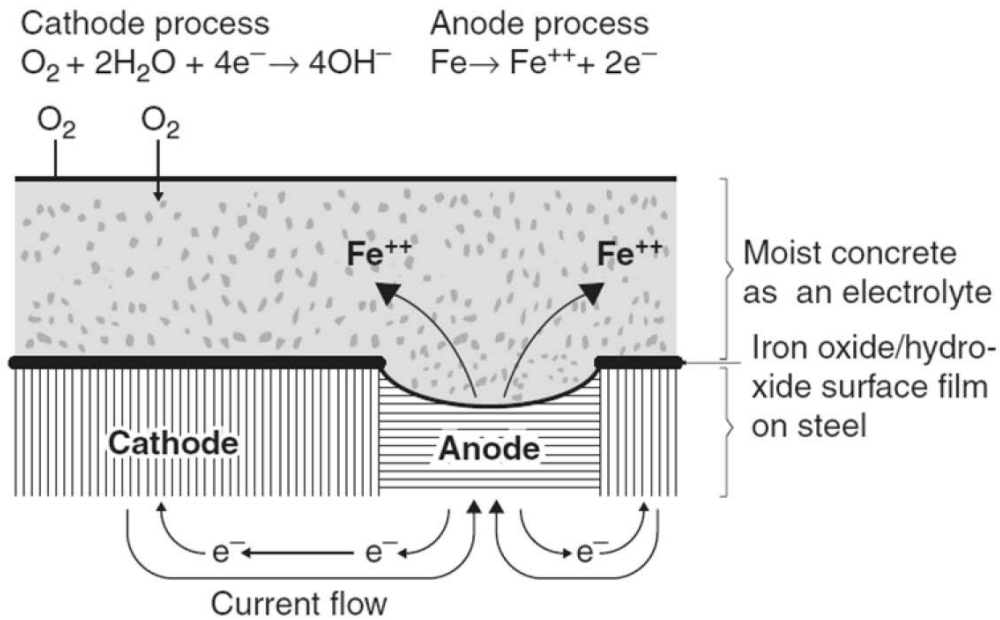


**Figure 2.1** Corrosion process in reinforcing steel bar [36]

### 2.1.1 Time to corrosion

Jensen et al performed a series of experiments to measure the chloride ingress in the cement and mortar paste [24]. In their study, it was determined that the ingress of chlorides follows Fick's law of diffusion, shown in Eq. 2.1. Stewart et al solved Eq. 2.1 in terms of the chloride ion concentration ( $C(x, t)$ ), distance from concrete surface ( $x$ ), time of exposure to chloride ions ( $t$ ), and the chloride diffusion coefficient ( $D_c$ ). The solution rendered equation Eq. 2.2 which describes the time to initiation of corrosion [50][58][53]. Mean values for  $C_0$  and  $C_r$  have been previously defined for environments that are controlled by deicing salts [18][56][12].

$$\frac{\partial C(x, t)}{\partial t} = D_c \frac{\partial^2 C(x, t)}{\partial x^2} \quad (2.1)$$

$$T_{corr} = \frac{x^2}{4D_c} \left[ erf^{-1} \left( \frac{C_0 - C_{cr}}{C_0} \right) \right]^{-2} \quad (2.2)$$

### 2.1.2 Rate of corrosion

Vu et al developed an empirical model to evaluate the corrosion rate [55][50]. In their study a constant corrosion rate was assumed. However, it is known that the corrosion rate is not constant over time because it is dependent on factors such as the quality of concrete, the amount of oxygen available in the environment, and the relative humidity. Nonetheless, for long term studies this approximation is valid. The underlying assumptions of this model are a relative humidity of 75% and a temperature of 20C. The model developed by Vu et al is shown in Eq. 2.3. Figure 2.2 shows the corrosion rate for different concrete covers ( $d_c$ ), as a function of the water to cement ratio ( $w/c$ ). In general, for large values of cover depth the rate of corrosion decreases rapidly, and as the water to cement ratio (i.e. lower quality concrete) increases the rate of corrosion increases.

$$i_{corr} = \frac{37.5(1 - w/c)}{d_c} \quad (2.3)$$

In addition, Vu et al further improved the model of corrosion growth in reinforcing steel developed by Stewart et al [55][50][9][18]. Their proposed model describes the reduction in diameter of reinforcing steel ( $d_{corr}(t)$ ) as a function of time described in Eq. 2.4. Figure 2.3 shows this model applied to a rebar with an initial diameter ( $d_{bi}$ ) of 3/4 inch, a concrete cover of 1-1/2, and water to cement ratios ranging from 0.36-0.50.

$$d_{corr}(t) = d_{bi} - \frac{1.0508(1 - w/c)}{d_c} (t - t_{corr})^{0.71} \quad (2.4)$$

Further, the evolution of corrosion in reinforcing steel can be expressed in the percent loss of mass of a rebar. If uniform corrosion is assumed, this can be expressed as the percent of reduction of diameter. The corrosion level can be expressed as shown in Eq. 2.5.

$$CL = \frac{d_i - d(t)}{d_i} * 100 \quad (2.5)$$

Combining Eq. 2.4 with Eq. 2.5, the variation of the corrosion level can be described as a function of time. Figure 2.4 shows the results of this process.

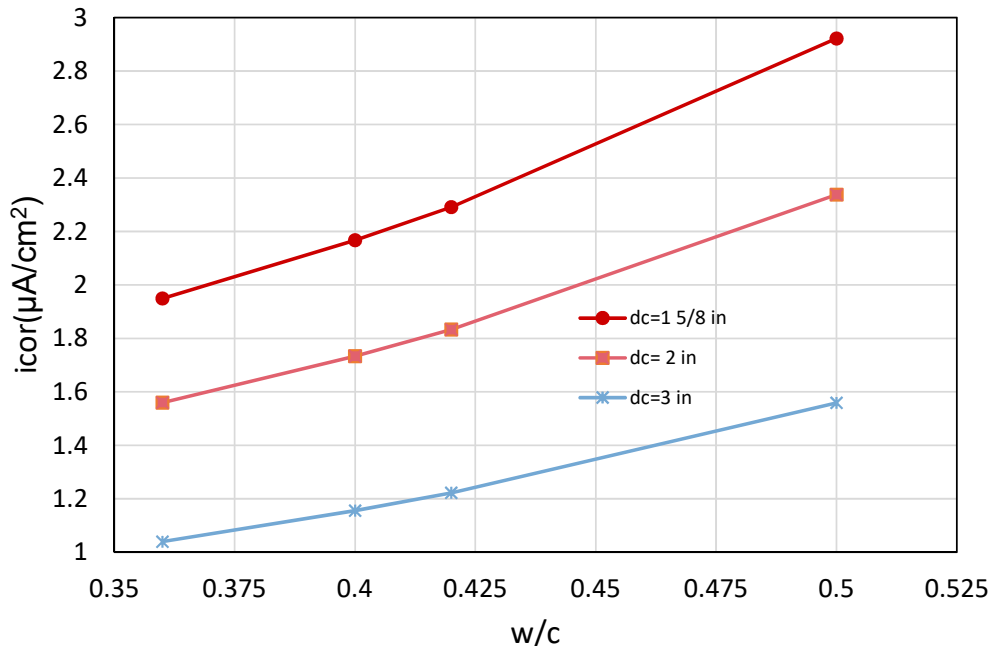


**Figure 2.2** Concrete water to cement ratio vs rate of corrosion

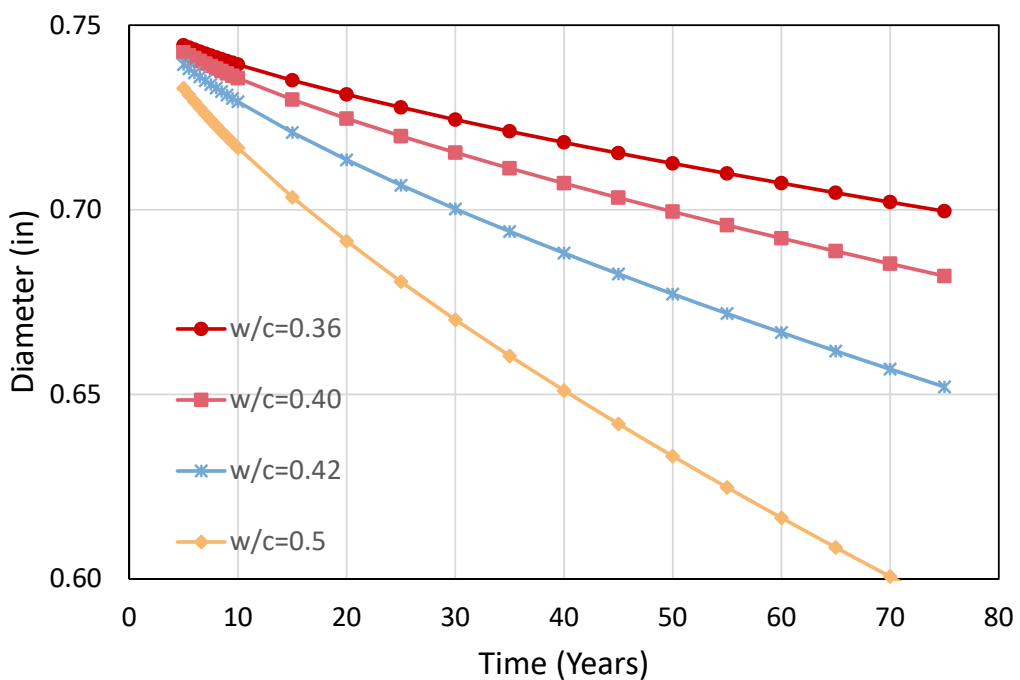


**Figure 2.3** Diameter decrease due to corrosion

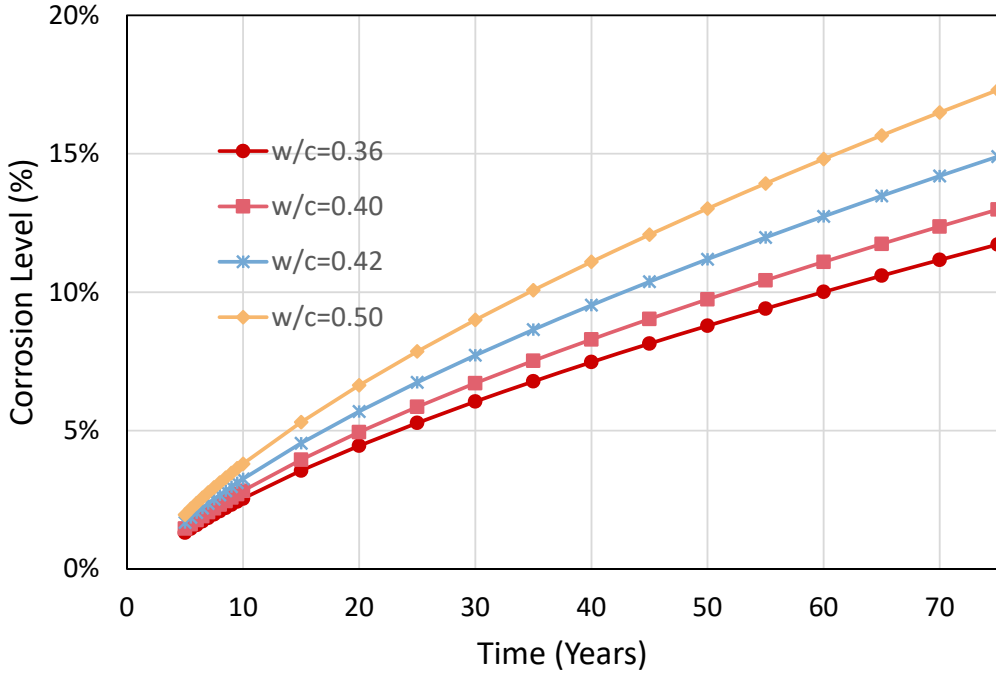


**Figure 2.4** Corrosion level vs time (years)

### 2.1.3 Corrosion modified properties of reinforcing steel bars

Yuan et al [61] performed tension tests on corroded rebars and determined that the mechanical properties of steel change with the level of corrosion. In general, as corrosion increases, the yield strength and ultimate strength of the reinforcing steel decrease. The variation of the mechanical properties is shown in Eq. 2.6 for the yield strength and ultimate strength of the reinforcing steel.

$$f_{y,C} = f_{yo}(1 - 0.021C) \quad (2.6)$$

$$f_{u,C} = f_{yo}(1.018 - 0.019C)$$

One of the limitations in their study is that the accelerated corrosion process used to develop the corrosion in the rebars did not account for the depassivation process that naturally occurs in rebars embedded in concrete. Chapter 3 shows a proposed experimental assessment that will provide an accurate evaluation of the mechanical properties of corroded reinforcing steel.

#### 2.1.4 Physical test on corroded RC Structures

Recent studies [29], [35] and [59] have been developed to assess the effect of corrosion in the structural performance of cantilever RC columns. These columns were subjected to accelerated corrosion to obtain different corrosion levels ( $CL$ ). The range of  $CL$  for these studies correspond to  $CL = 0\% - 20\%$ . In these studies the accelerated corrosion was performed via an electrochemical process directly applied to the reinforcing steel as shown in Fig. 2.5.

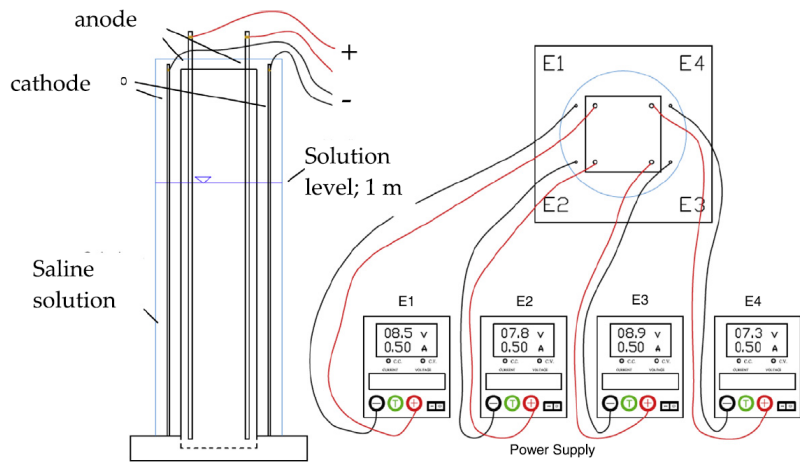


**Figure 2.5** Force displacement response of RC corroded columns [35]

The corroded RC columns were then subjected to a quasi-static loading protocol. The resulting force displacement response of one of these experiments is shown in Fig. 2.6. It can be seen that there is a reduction of the strength and displacement capacity of the system.

As stated in the previous section the mechanical properties of steel are affected by corrosion. In the previous studies [35] the authors performed tension tests on corroded reinforcing steel. In these tests a reduction in the mechanical properties of steel was observed as well as a reduction in the rupture strain  $\varepsilon_{srup}$ , see Fig. 2.7.

While these studies show how corroded RC columns behave under cyclic loading, they did not consider the generation of the protective film due to the alkaline environment of the concrete. This film can modify the mechanical properties of corroded steel. In addition, the accelerated corrosion process used a 3%  $NaCl$  concentration solution while the chloride attack in concrete usually has a 1.0% - 1.5% concentration of the same chloride. Therefore the results obtained from these studies do not accurately represent the actual conditions of corroded RC columns. Thus,

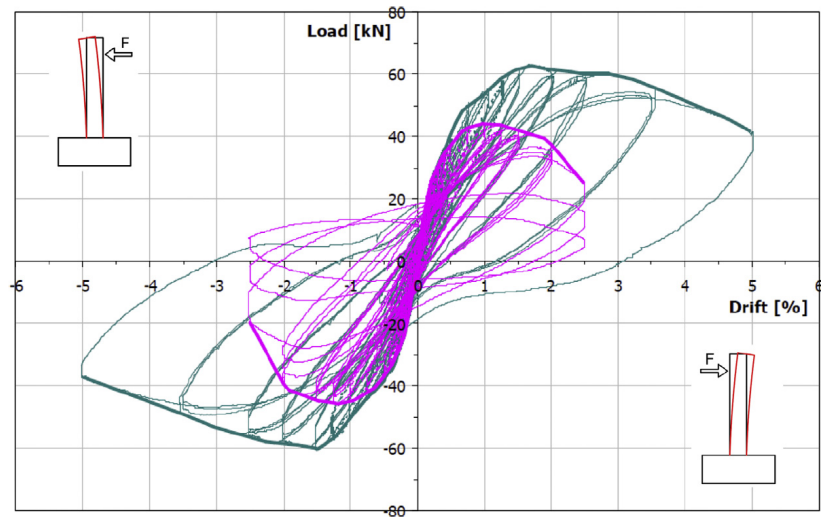


**Figure 2.6** Corrosion process for RC column [35]

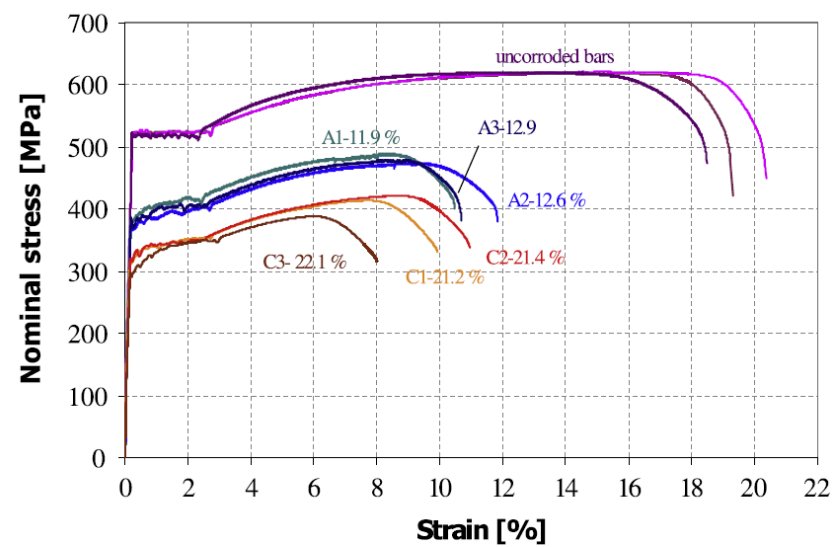


**Figure 2.7** Corroded rebars stress-strain curves [35]

an experimental campaign is proposed that will provide results on the mechanical behavior of corroded reinforcing steel inside concrete. The experimental campaign is discussed in Chapter 3.

## 2.2 Steel strain aging

While corrosion is an important parameter that affects steel in structures, strain aging is a phenomenon that affects mild steels, which are common in older structures. Strain aging is the process in which steel after being subjected to large strains and an amount of time passes after the loading, when the steel is reloaded it presents a higher strength and reduced ductility than before the first loading. Therefore the incorporation of this parameter in this research will help evaluate this effect in older structures when subjected to repeated earthquake loading. This process is explained in more detail in this section.

### 2.2.1 Metallurgical process

It is generally accepted that strain aging is due to the diffusion of carbon and/or nitrogen atoms in solution to dislocations that have been generated by plastic deformation. Initially, an atmosphere of carbon and nitrogen atoms is formed along the length of a dislocation, immobilizing it. Extended aging, however, results in sufficient carbon and nitrogen atoms for precipitates to form along the length of the dislocation[41][23].

These precipitates impede the motion of subsequent dislocations and result in some hardening and loss in ductility. The extent of strain aging, which is a thermally activated process, depends primarily on aging time and temperature. In general, extended aging results in a saturation value above which further aging has no effect [45].

A second strengthening mechanism occurs when cold deformation (alone) is applied to steels. When dislocations break away from their pinning interstitial atoms and begin the movement causing slip they begin to intersect with each other. A complex series of interactions between the dislocations occurs, causing them to pin each other, decreasing their mobility. The decreased mobility also results in higher strength, lower ductility and lower toughness. As a result, cold deformed steels already have lowered ductility and toughness before any strain aging occurs. When heating follows cold deformation, the loss in ductility and toughness is greater. It is this combination of events that is the most damaging to the toughness of structural steels [38].

### 2.2.2 Strain aging effects in structures

Strain aging is the process by which steel after being subjected to large strains, develops an increased strength and reduced ductility with time. Large earthquakes can cause this effect on structures built with mild steel. Therefore, it is important to include strain aging in a time dependent analysis. Furthermore, strain aging will cause an increase in the strength of the plastic hinge and as a consequence plastic hinges may form in regions of the structures that have not been designed for such demands. The effects of strain aging may also alter the transverse reinforcement due to cold bending, making them susceptible to brittle failure[38].

According to Restrepo-Posada[45], most strain aging occurs in the first 37 days. In addition, Momtahan et al [38] studied strain aging effects with respect to time at different levels of pre-strains. The pre-strains ranged from  $2\varepsilon_y$  to  $10\varepsilon_y$ , for a time frame of 3 days to 50 days. Their results determined that a significant effect of strain aging took place from pre-strains  $5\varepsilon_y$  and on. Strains higher than  $15\varepsilon_y$  indicate a performance level in which substantial damage has been induced in the structure such that it is deemed unrepairable and therefore pre-strains higher than  $15\varepsilon_y$  are impractical and were not studied [38].

Momtahan et al correlated the increase in yield strength as a function of time and the pre-strain in reinforcing steel bars. The proposed equations are shown below:

For  $10\varepsilon_y$

$$\frac{f_y}{f_{yi}} = 0.0026t + 0.9838 \quad (2.7)$$

For  $5\varepsilon_y$

$$\frac{f_y}{f_{yi}} = 0.0008t + 0.996 \quad (2.8)$$

For  $2\varepsilon_y$

$$\frac{f_y}{f_{yi}} = 0.0004t + 0.9979 \quad (2.9)$$

It is proposed to limit the increase in yield strength obtained at 50 days, which was the limit of scope of their study. Equations 2.7 to 2.9 are plotted in Fig. 2.8

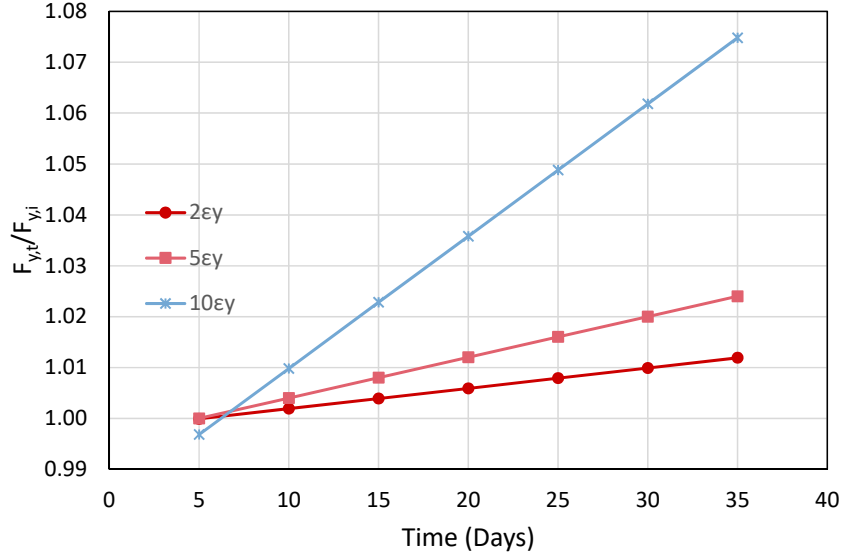


**Figure 2.8** Strain aging effect on yield strength vs time (days)

## 2.3 Damage Indexes

The use of damage indexes has dominated the research related to damage accumulation. While these methods are practical and appear to have a logical basis, they are based on empirical relationships and need to be correlated for each structure case to be of any significance. An example is shown in this section demonstrate this inconsistency. The literature review presented here is to understand what has been done previously to study the effect of damage accumulation, however it is the purpose of this research that strain limit states are an improved measure of damage over empirical methods.

The effect of cumulative damage in structures was studied by Park and Ang (1985) [60] in their study the authors proposed the damage index as shown in Eq. 2.10. The damage index was used as a measure to quantify damage in terms of the maximum experienced earthquake and the absorbed hysteretic energy.

$$D = \frac{\Delta_m}{\Delta_u} - \beta \frac{E_h}{F_y \Delta u} \quad (2.10)$$

$\Delta_m$ : Maximum deformation under earthquake

$\Delta_u$ : Ultimate deformation under monotonic loading

$F_y$ : Calculated yield strength

$E_h$ : Total hysteretic energy

$\beta$ : Dimensionless constant

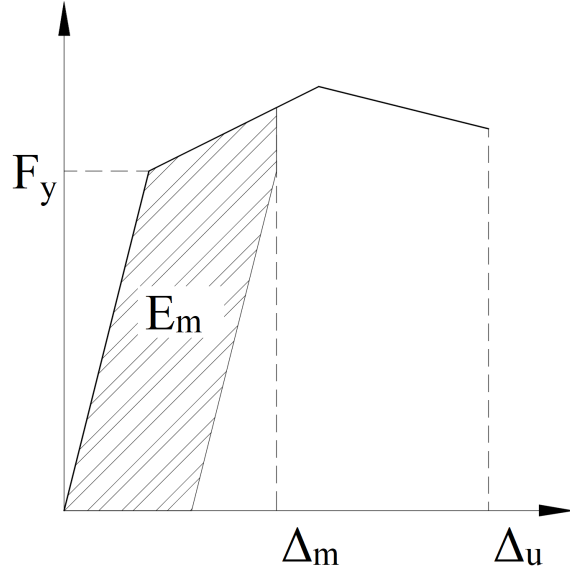


**Figure 2.9** Park and Ang conceptual scheme

Equation 2.10 was derived for concrete elements. The first term here is a simple, pseudo-static displacement measure. The second term accounts for cumulative damage. This concept is shown in Fig. 2.9. The advantages of this model are its simplicity and flexibility in adapting the model to correlate with experimental data. After calculating the damage index, this can be classified according to the damage index level defined by Park and Ang [60]. The damage index level classification is shown in Table 2.1.

**Table 2.1** Damage index level classification [60]

Level	Damage index (DI)	Damage measure
I	$DI < 0.1$	No damage; localized minor cracking
II	$0.1 < DI < 0.25$	Minor damage; light cracking throughout
III	$0.25 < DI < 0.4$	Moderate damage; severe cracking; localized spalling
IV	$0.4 < DI < 1.0$	Severe damage; crushing of concrete; reinforcement exposed
V	$D > 1.0$	Loss of elemental load resistance

However, this model has several limitations. Firstly, the calibration of the  $\beta$  coefficient with observed damage has proven to be very low ( $\beta = 0.05 - 0.15$ ) [60] [19], rendering the second term relatively inconsequential compared to the contribution of the first term. A sample result is taken from Gosh et al [19], which applied a modified version of the Park and Ang damage index in terms of the moment ( $M_y$ ), the rotation ( $\theta_y$ ), and curvature ductility ( $\mu$ ). The modified model is expressed in Eq. 2.11.

$$D = \frac{\mu_m}{\mu_u} - \beta \frac{E_h}{M_y \theta_y \mu u} \quad (2.11)$$

Using the following values:  $\mu_m = 4.93$ ;  $\mu_u = 17.02$ ;  $M_y = 8751.375$ ;  $\theta_y = 0.0042$ ;  $E_h = 119.07$ ;  $\beta = 0.05$

And substituting in equation Eq. 2.11:

$$D = \frac{\mu_m}{\mu_u} - \beta \frac{E_h}{M_y \theta_y \mu u} = 0.3$$

**First term:**

$$\frac{\mu_m}{\mu_u} = \frac{4.93}{17.02} = 0.2897$$

**Second term:**

$$\beta \frac{E_h}{M_y \theta_y \mu u} = 0.05 \frac{119.07}{8751.375 * 0.0042 * 17.02} = 0.0103$$

It can be seen that 97% of the damage index comes from the first term, which is the elastic term, and the inelastic part is only 3% of the total.

Despite its limitations, several studies have used or modified this model to study the effects of cumulative damage for different structures. Those of relevant importance are those performed by Kunnath et al [28], who used a modified Park and Ang model, to account for damage at the local level for elements in the structural analysis program IDARC 3.0. In this software, for the case of multiple degrees of freedom buildings they also added parameters to consider the damage at the inter-story level and the global model. Ghosh et al [19] developed a damage accumulation framework to estimate the probability of exceeding a damage index for multiple ground motions. Other regressions have been proposed [25], [13], [46] but show no improvement in assessing the damage state of a structure. While these studies provide an insight into some of the characteristics of damage accumulation they, still rely on the Park and Ang model and therefore carry the same limitations.

Krawinkler (1987) [26] proposed a method that considered damage as a function of low cycle fatigue parameters. The form of the Krawinkler damage index for steel components,

weldments, and local buckling has a general shape of the Miner model. This model relies on the accumulation of plastic deformations. While this model has proven to work well for the evaluation of individual steel structure elements, it does not provide a way to generalize damage for other types of structures.

## 2.4 Multiple earthquake loading

The evaluation of multiple seismic events has been scarcely studied; however, their effects have been felt in numerous earthquake sequences such as the Christchurch 2010, Umbria-Marche Earthquake 1997 and the Puerto Rico Earthquakes 2020. The hypothesis is that accumulation of damage will restart in a smaller seismic event to achieve a prescribed limit state, similar to how corrosion and other aging phenomena might impact the intensity needed to achieve a future limit state.

In the literature the study of multiple earthquake loading can be classified in two groups:

- Mainshock-aftershock sequences
- Mainshock sequences

These studies have shown what are some of the effects of multiple earthquake loading for different structures.

### 2.4.1 Mainshock-aftershock sequences loading

Strong aftershocks can increase the state of damage of a building or even collapse an already damaged structure. It is therefore important to quantify the increase of seismic demands in structures due to aftershock loading. In recent years different studies have been carried out to develop methodologies that consider these effects.

Tesfamariam et al [52] investigated the increase in the demands for multiple degrees of freedom systems (MDOF). They conducted a parametric study of RC bare frame buildings and RC frame with infill masonry buildings. The main parameter of study focused on the thickness of the infill frames ranging from 75mm - 125 mm. In addition, a series of mainshock-aftershock sequences were applied, selected for the area of Vancouver, BC. The mainshock-aftershock sequence were selected using the conditional mean spectra (CMS) over the period range of the structures. The motions considered in their study were different for the bare frame and the infill frames. The bare frame was subjected to a mainshock followed by three aftershocks, while those of the infill frame consisted of one mainshock followed by one aftershock each. Their

results showed that there is an increase of 10% in the inter-story drift demands for the RC bare frame structures. For the case of infill frames the inter-story drift did not significantly increased. Their study used FEMA 356 [14] to define the performance limit states. FEMA 356 drift performance limit states are based on linear regression on observed damage to drift level obtained from experimental tests. The linear regression compared to the experimental results have high dispersion. Therefore, it is possible that in the study by Tesfamariam et al, that while a drift limit state did not increase after applying a MS-AS sequence, a higher strain was reached in some of the components due to the MS-AS sequence, and as consequence a higher strain performance limit state could have been reached. Thus emphasizing the importance of using strain performance limit states. Similarly, Raghunandan et al [44] studied the vulnerability of RC frame structures. Their study showed that depending on the level of interstory drift achieved during the mainshock the additional damage experienced during the aftershock will be different. For example, the authors showed that for an RC frame that experiences 4% or more interstory drift in the mainshock, the median capacity to resist aftershock shaking is reduced by about 40%. Furthermore, other studies have focused on the behavior of single degree of freedom (SDOF) systems response to mainshock-aftershock (MS-AS) sequences [22][32]. Hatzigeorgiou et al focused on determining the inelastic displacement coefficient variation due to the MS-AS sequence. Their study concluded that there is an increase in the inelastic displacement demands, however, the limitations in their study did not report what happens to the performance limit states. Further, Manafpour et al studied the seismic drift behavior of structures to MS-AS sequences for far-field earthquakes and near-field earthquakes. Their study concluded that for SDOF structures near-field earthquake sequences were the most damaging, increasing the drifts by as much as 45% compared to a structure subjected to the main shock only.

Researchers have applied two earthquake selection procedures for mainshock-aftershock sequences. The first method, incremental dynamic analysis (IDA), consists of 1)subjecting the nonlinear building model to a ground motion having a particular intensity, 2) recording the response of the structure [54], 3)in successive analyses, the ground motion is incrementally scaled to a higher intensity measure (IM), and 4)the structural response is recorded in each analysis. The IDA procedure was extrapolated to for MS-AS sequence as follows: 1)Apply the IDA to the mainshocks to obtain 11 drift damage levels ranging from 0.5% to 5.5% of interstory drift in the structure, 2) after each mainshock include an incrementally scaled aftershock with a 4 seconds gap between the mainshock and the aftershock, and 3)Change the polarity of the aftershock, which refers to the direction of the aftershock variation to the mainshock. Fig. 2.10 shows one of the resulting MS-AS sequences using the IDA methodology. Due to the use of scaling factors the IDA methodology uses artificial mainshock-aftershock sequences. In addition, the IDA analysis

can be computationally expensive. For instance, the authors reported a total of 9900 ground motion sequences per structure.

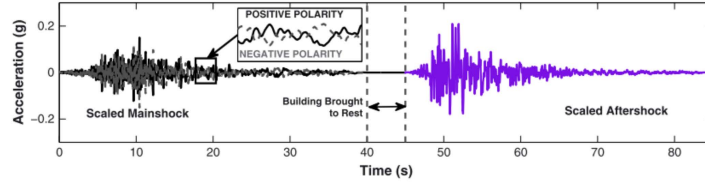


**Figure 2.10** Mainshock-aftershock sequence train of ground motions [44]

The second method consists of matching the MS-AS sequences to a site seismic hazard curve obtained from a probabilistic seismic hazard analysis (PSHA). Tesfamariam [52] used conditional mean spectra (CMS) to match and select mainshock-aftershock sequences for structures located in Vancouver, BC. Their study selected MS-AS sequences from two databases of ground motions, NGA-West2 [2], and the K-NET//KiK-net [39]. The CMS process consists of computing the expected response spectrum associated with a target spectral acceleration ( $S_a$ ) value at a single period, using the known values from PSHA such as the magnitude, distance, and  $\epsilon$  values. In their study the authors used CMS to select the MS-AS sequences for different earthquake scenarios a)Crustal earthquake, b) Interface, and c) Inslab. They hypothesized that different earthquake scenarios would have different MS-AS sequence characteristics such as higher spectral acceleration ( $S_a$ ) values at short periods for interface earthquakes, and high  $S_a$  values at longer periods for crustal earthquakes. They argue that using the CMS method makes the selection of ground motion consistent with the seismological features of the area of study. Fig. 2.11 shows this selection for a structure with a 0.4s period for crustal earthquakes. The CMS method adapts to the site conditions, no scaling of MS-AS is required since the selection is optimized to ground motion sequences stored in the databases. Since the CMS method uses site-specific data, it can be a part of an analytical framework that can be adapted to different seismic regions.

#### 2.4.2 Mainshock sequences loading

Reliable temporal prediction of earthquakes is currently impossible. However, for a large region, earthquakes recurrence time can be modeled reasonably well as a Poisson process. Sunasaka [51] developed mainshock sequences that followed a Poisson process. Their study focused on the

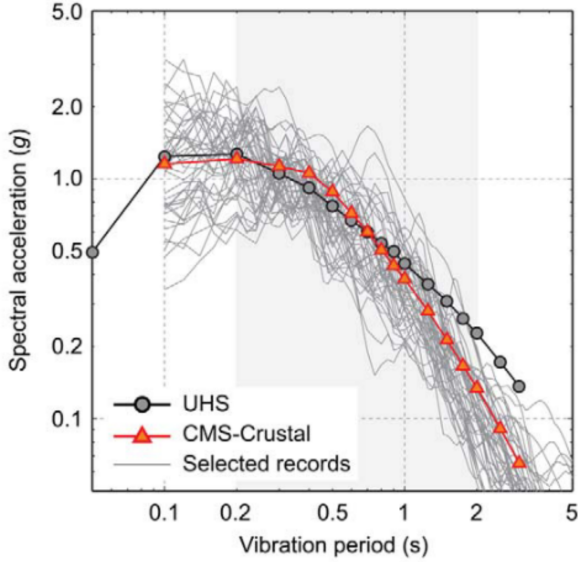


**Figure 2.11** Mainshock-aftershock sequence selection at  $T=0.4\text{s}$  for crustal earthquakes in Vancouver, British Columbia [52]

accumulation of damage due to mainshock sequences, and mainshocks-aftershocks sequences. Damage accumulation was accounted for by the Park and Ang index. The authors used ground motion prediction equations to develop artificial mainshock sequences. Their study calculated the recurrence period, magnitude, location and peak ground acceleration for each of the mainshocks. The author subjected an SDOF bridge in Eureka, CA to the mainshock sequence shown in Fig. 2.12. While the results shows a significant increase in the damage index due to mainshock sequences, the conclusions are limited by the assumption that a Poisson process can be applied to single faults, which has not shown good correlation with observed events[48]. While this study shows what could be possible if mainshocks were predictable in small regions, more advances in seismology are needed to confidently apply the proposed methodology.

Other studies have used three equally spaced mainshocks [22]. The three equally spaced mainshocks can be deployed without much computational effort, however, there is not a seismological basis for the use of three equally spaced mainshocks. Therefore, the use of this methodology would be limited to a scenario analysis and not useful for analysis and design, since the probabilities of three equally spaced in time mainshocks on any given structure is very low.

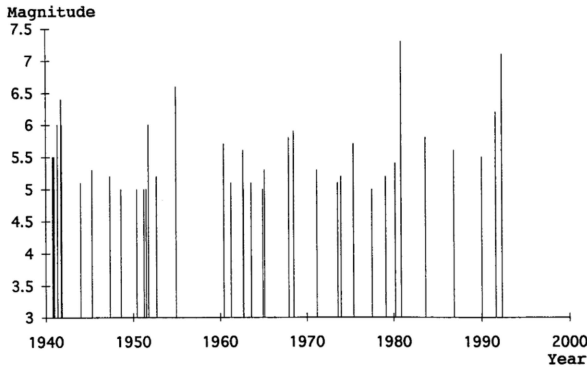


**Figure 2.12** Mainshock sequence selection at Eureka, CA [51]

## 2.5 Aging of structures

There have been attempts by many researchers to characterize the aging of structures.

In recent years studies have focused on the effect of cumulative damage. These studies have focused on assessing the damage accumulation considering multiple earthquakes, corrosion and service life of the structure. Two field of study have been observed:

- Probabilistic framework
- Fragility curves

### Probabilistic Framework

One of the most widely used probabilistic frameworks is the Pacific Earthquake Engineering Research Center (PEER) Performance Based Design (PBD). PEER PBD can be expressed by the following equation:

$$\nu_{DM}(dm^{LS}) = \iint D_{DM|EDP}(dm|edp)|, dG_{EDP|IM}(edp|im)|| d\nu_{IM}(im)| \quad (2.12)$$

Mackie et al [30] using the PEER PBD, developed the performance based damage design (PBDD) and performance based loss design (PBLD) by defining the probabilistic demand, damage, and loss model parameters in terms of reinforced concrete column damage. The RC column damage was defined in terms of mean drift ratios obtained from the PEER structural performance database (<http://nisee.berkeley.edu/spd/>). The drift limit states considered in their study were concrete spalling, bar buckling and failure. In their study, failure was defined

as the first occurrence of the database fields for reinforcing bar fracture and loss of axial load-carrying capacity

The authors show that for a given intensity measure ( $IM$ ) and a confidence level of achieving a limit state, it is possible to then define the probability of exceeding that limit state. The authors used peak ground velocity ( $PGV$ ) as their intensity measure. While this methodology was able to define damage and incorporate it into the PEER PBD framework, the authors did not consider strain to define the limit states. In a PEER report Mackie et al studied seismic demands for performance-based design of bridges. In the report they performed a design parameter sensitivity analysis in which they evaluate different intensity measures. Their analysis showed that the optimal  $IM$  to predict most engineering demand parameters ( $EDP$ ) is the first mode spectral displacement  $S_d(T_1)$  [31]. However, at the time their report was written the  $S_d(T_1)$  did not show good correlation with strain as the  $EDP$ , and as a consequence they did not recommend to use strain as a predictor of structural performance. Nonetheless, a recent study presented by Krish et al shown that new advancements in the modeling of plastic hinge forming members can more accurately relate strain and  $S_d(T_1)$ . They conclude that the use of these parameters is well suited to predict the performance of structures [27].

### Fragility Curves

Another common trend in this subject is the use of fragility curves to estimate the effect of damage in structures. Two main approaches were found in the literature. One of them relied on the Park and Ang Model damage index to define damage, while the second approach related damage to drift.

Ghosh et al [19] formulated a damage accumulation framework. Their study relied on the Park and Ang Damage index explained in the previous section. The study performed a series of nonlinear time history analyses for two cases:

- Using a constant main shock hazard occurrence rate (3 main shocks in a 50-year period)
- Mainshock - Aftershock series using a time-dependent aftershock hazard occurrence rate

The results from their study showed regression equations that statistically predict the damage index as a function of earthquake intensity and damage history. This study revealed that for both mainshock and aftershock scenarios there was a significant increase in the probability of damage index exceeding a damage index level (as defined in Table 2.1) under repeated shock scenarios. While this study shows the importance of considering damage accumulation, these results have to be taken with caution, since they present the same disadvantages as the Park and Ang damage index.

Ghosh et al [18] also studied the effects of corrosion on time dependent seismic fragility curves. Their study characterizes corrosion in concrete columns as a continuous phenomenon that occurs as a function of time. The authors also considered the effects of corrosion on steel bridge bearings. The authors then ran a series of NLTHA analyses for different aging times of the structures. Based on their analysis, time dependent fragility curves were presented. The results showed that as time increases, and corrosion increases as a consequence, the probability of exceeding a limit state increases. In their study, limit states were defined on the basis of inter-story drifts which were obtained from experimental results and field observations [42]. It is important to mention that the limit states used in their study were not defined on the basis of strains or other structural property. Instead the limit states came from a survey performed in central and southeastern United States departments of transportation, on the premise of a range of experienced inter-story drifts and the time taken to repair them. In addition, assuming that corrosion is a continuous process has to be cautiously taken as valid. This is because site information such as temperature, water to cement ratio, the addition of cementitious materials such as silica fume, and the environment (e.g. coastal vs inland) affect the rate of propagation of corrosion[53].

While these studies provide a general view on how damage increases the likelihood of observing collapse or deterioration of the seismic performance, the methods used to arrive at those conclusions can be misleading since the definition of damage as either a Damage Index or Drift are not the best parameters to quantify the damage. It is our belief that strain-based limit states will provide a better understanding of the implications of damage accumulation.

## 2.6 Research Gap

Many studies have tried to show the importance of quantifying the effects of accumulated damage and multiple shocks throughout the lifetime of a structure. Therefore, it is important to develop a model that establishes the likelihood of achieving a limit state as the structure ages. In addition, it is important to understand the impacts of aging on bridge seismic performance. Furthermore, bridges in seismic areas can be subjected to main shock and aftershocks. Therefore, a methodology that incorporates both aging and multiple seismic events is needed.

Damage accumulation is a topic that has been gaining momentum in the engineering community, this study will better inform the potential future conditions of a structure to stakeholders such as state DOTs, building owners, and practicing engineers. In the literature it was observed that damage accumulation has been studied using the Park and Ang damage index or drift-based limit states to measure damage accumulation. Different researchers have also included

corrosion into their scope of analysis, which shows that aging conditions play an important role in the deterioration of a structure. In addition, Krish [27] determined that spectral displacement at first effective period is an improved intensity measure (IM), while the past literature used the peak ground acceleration (PGA) as the controlling IM. This research will develop a parametric study using a series of single degree of freedom (SDOF) systems, subjecting them to different conditions such as corrosion, and steel strain aging. The SDOF structures will be subjected to a sweep of ground motions using nonlinear time history analysis to obtain maximum strain demands. With the results from NLTHA, fragility functions will be used to show the increase in the likelihood of reaching a performance limit state due to aging of the structure. In addition, this research will provide the engineering community with a design framework to account for damage accumulation in their analysis and guide decisions on the resiliency of a structure. In addition, this study will provide a methodology in which the Direct Displacement-Based Design (DDBD) is modified to consider the effects of damage and aging conditions.

### 2.6.1 Objectives

The main goal of this research is to provide a design methodology to consider damage for performance based seismic design of structures. In addition, this study will demonstrate the implications of aging conditions and multiple earthquakes for the design of bridge RC columns.

- Incorporate different aging conditions and develop fragility curves that considers strain limit states as a measure of damage
- Establish limit states for corroded rebars
- Inform the research community of the necessary methodology to appropriately mimic real corrosion process in material experiments of corroded rebars, which can later be extrapolated to large scale testing of RC columns subjected to corrosion
- Consider the effects of multiple earthquakes for two cases: (1) Mainshock-Aftershock sequence, and (2) Mainshock-Aftershock sequence with the effects of time between the mainshock and the aftershock.
- Incorporate these results into the Direct Displacement Based Design (DDBD) methodology, through the use of factors that correspond to the aging conditions

# **Chapter 3**

## **Experimental phase: mechanical properties and performance of corroded reinforcing steel**

The experimental portion of this research program consists of a total of 54 buckled bar tension tests using the method proposed by Barcley et al [5]. The experimental phase of this research aims at studying the effects of depassivation in the modified mechanical properties of corroded grade 80 reinforcing steel, and the modification on the bending strain in corroded buckled bars. This chapter outlines the rebar preparation, experimental setup, instrumentation, and expected results.

### **3.1 Proposed experimental campaign**

As explained in the previous section the steel inside concrete generates a protective film due to the alkaline environment generated by the cement paste. During a chloride attack, when chloride contact the surface of the steel, the protective film starts to be eliminated, this process is known as depassivation. The proposed experimental campaign aims at simulating the process of corrosion as it would occur in a rebar embedded in concrete. The experiment process is outlined here:

1. Passivation of the reinforcing steel
2. Accelerated corrosion of reinforcing steel

3. Tension tests
4. Buckled bar tension (BBT) test

### **Passivation of reinforcing steel**

Methods to generate the passive film on the reinforcing steel surface are available in the literature [17]. According to this study, it is possible to generate the passivation process in the same way as it occurs in reinforcing steel embedded in concrete by using an alkaline porous solution. The authors, studied ten different porous solutions, out of which five had all the alkali oxides that exist in the cement. Of these five solutions, the one that showed better performance in the quality of the protective oxides grown on rebar is shown here with its corresponding concentrations:

- Saturated calcium hydroxide  $Ca(OH)_2$
- Sodium hydroxide  $Na(OH)$  (4.00 g/l)
- Potassium hydroxide  $(OH)$  (11.22 g/l)
- Calcium sulfate dihydrate  $Ca(SO)_4 + 2H_2O$  (13.77 g/l)

This is the solution that will be used in this research to generate the passive film on the specimens. To generate the passive layer of the reinforcing steel, the rebars will be placed in the pore solution for a minimum of 8 days. Anodic polarization tests will be performed on the rebars to determine the passive current density. A figure of this process is shown in Fig. 3.1. In addition, the ends of the rebars will be protected to prevent corrosion in these zones of the specimens, the protection at the ends is based on the standard ASTM G109-07 with some alterations. Figures Fig. 3.2 and Fig. 3.3 show the specimen geometry and the preparation of the ends of the rebars.

### **Accelerated corrosion of reinforcing steel**

The accelerated corrosion will be done by using a galvanic cell. Different studies [17] have shown that for rebars with passive films a concentration of 0.3 Moles of sodium chloride ( $NaCl$ ) will start the depassivation process on the rebars. In the study presented here, the specimens will be subjected to a current of 5mA equivalent to  $47\mu A/cm^2$ . This current is sustained for a period of time according to Faraday's Law until the desired level of corrosion is reached.

$$t = \frac{\lambda m_{loss} \eta_{specimen} C_{faraday}}{i M_{specimen}} \quad (3.1)$$

The corrosion levels, the current and the time of application is shown in Table 3.1.

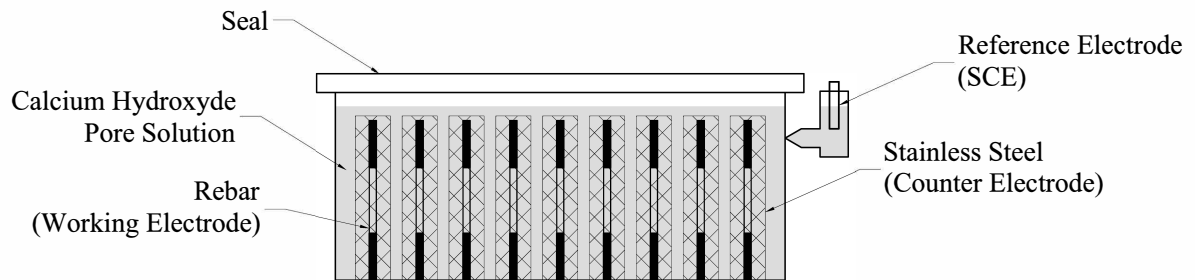


**Figure 3.1** Rebars Passivation Process in Calcium Hydroxyde Pore Solution

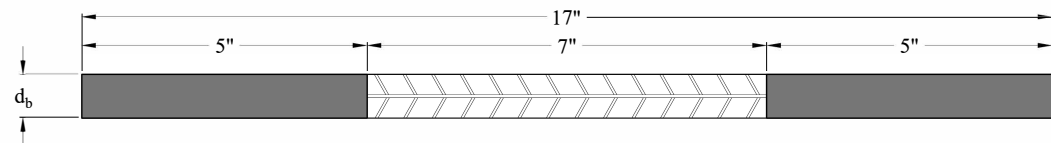


**Figure 3.2** Rebar Specimen Geometry

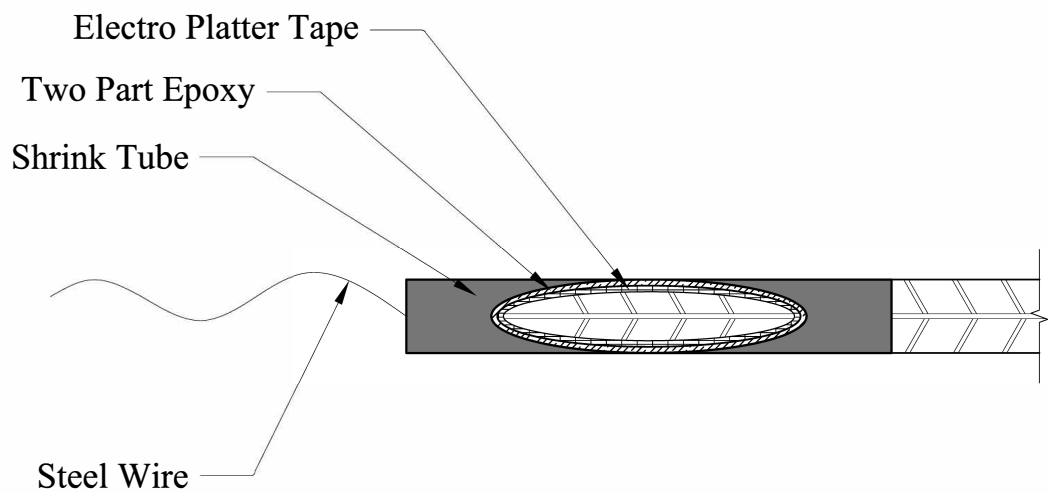


**Figure 3.3** Rebars Ends Protection

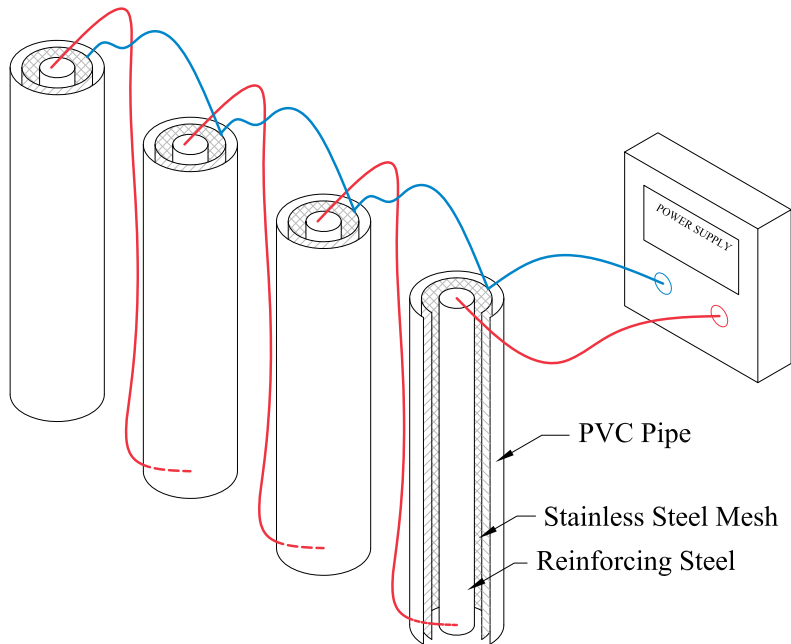


**Figure 3.4** Accelerated corrosion process

**Table 3.1** Accelerated corrosion times in 3/4" rebar

Corrosion Level (CL)	Mass loss (g)	time(days)
5%	1.12	9
10%	2.24	18
15%	3.36	27
20%	4.47	36
25%	5.59	45

## Tension tests

A series of tension tests will be performed according to ASTM A370. The main objective of this tests is to evaluate differences in the stress-strain behavior of corroded reinforcing steel. This will determine if there is any reduction in the ductility of steel for this condition.

### Buckled bar tension (BBT) test

One of the limit states that control performance-based design is buckling of reinforcing steel, recent tests have been developed to determine the critical bending strain of buckled reinforcing steel [5]. The buckled bar tension (BBT) test simulates bending and tension strain demands on a buckled bar, to determine critical bending strain in buckled rebars.

Barcley et al [5] developed a methodology to calculate local strains on a buckled bar using an LED optical sensor system [40]. The procedure is illustrated in Fig. 3.5.

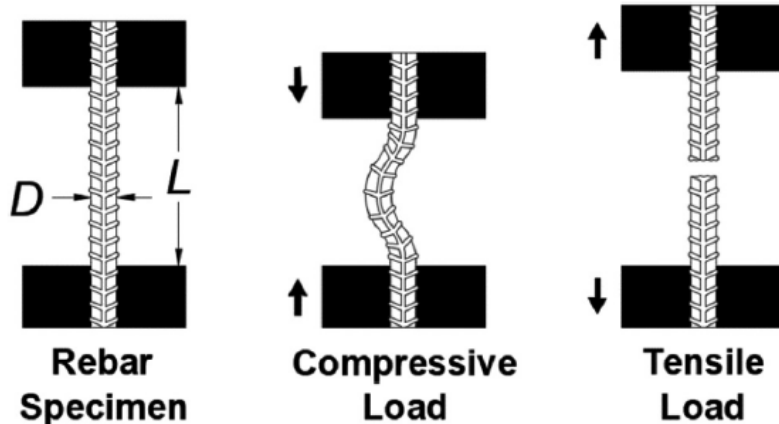


Figure 3.5 BBT Test sequence[5]

The procedure to perform the buckled bar tension test consists of:

1. First, place rebar in a univeral testing machine (UTM), and prepare the rebar specimen with LED markers on the surface of the specimen such that the displaced shape of the bar can be measured.
2. Second, compress the rebar specimen to impose a bending strain of a prescribed level. Barcley et al showed that a fourth order polynomial can be fit to the LED sensors near

the buckled region of the bar to obtain the displaced shape ( $w$ ). The bending strain is calculated using solid mechanics principles. Curvature is the second derivative of the displaced shape ( $w$ ) for small displacements is calculated as:

$$\phi = \frac{\frac{d^2w(x)}{dx^2}}{\left[1 + \left(\frac{dw(x)}{dx}\right)\right]^{\frac{3}{2}}} \approx \frac{d^2w(x)}{dx^2} \quad (3.2)$$

If we assume that the bending is symmetric for the rebar then the strain in the extreme fibers of the rebar is calculated as:

$$\varepsilon_b = \phi \left( \frac{d_{bl}}{2} \right) \quad (3.3)$$

Combining equations Eq. 3.2, and Eq. 3.3 then the bending strain can be expressed as:

$$\varepsilon_b = \frac{d^2w(x)}{dx^2} \left( \frac{d_{bl}}{2} \right) \quad (3.4)$$

An example of the calculation of the bending strain is shown in Fig. 3.6

3. Second, Once buckled to the prescribed curvature, the bar is loaded in tension until fracture is observed
4. Then the process is repeated with a different bar for a different bending strain. After all the tests are performed results from elongation at peak force can be generated as the example shown in Fig. 3.8. From the results obtained through BBT tests the critical bending strain can be determined. The critical bending strain is defined as the point at which a low elongation under load is obtained. This low elongation results in a brittle fracture of the rebar as shown in Fig. 3.7(b). Fig. 3.8 shows that for bars with rebars the critical bending strain is  $\varepsilon_b = 0.10$  for grade 80 ksi steel.

The BBT test is proposed for different levels of corrosion such that any changes on the behavior are studied and incorporated in the analytical model. The proposed test matrix is shown in Table 3.2. It must be noted that in each corrosion level for the BBT tests, each experiment will correspond to a different prescribed bending strain. The selection for each prescribed bending strains consists in 1) Start with the maximum bending strain determined in previous research to be around  $\varepsilon = 0.10$  as shown in Fig. 3.8, 2) if brittle fracture is observed the next test will be at a lower bending strain for example  $\varepsilon = 0.08$ , 3) otherwise higher strains such as  $\varepsilon = 0.12$  will be evaluated, this is repeated for each corrosion level. It is expected that

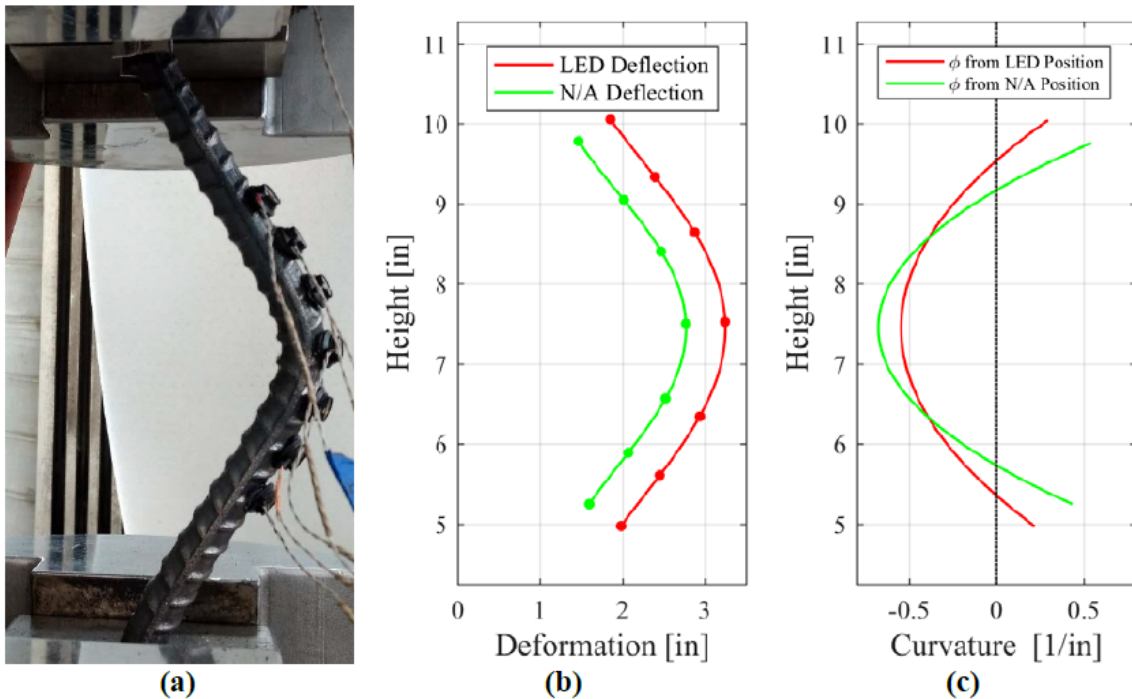


**Figure 3.6** a) Picture of buckled bar; (b) Position of optical markers and adjustment to neutral axis;  
 (c) Calculation of curvature [4]



**Figure 3.7** (a) Ductile rebar fracture; (b) Brittle rebar fracture [4]

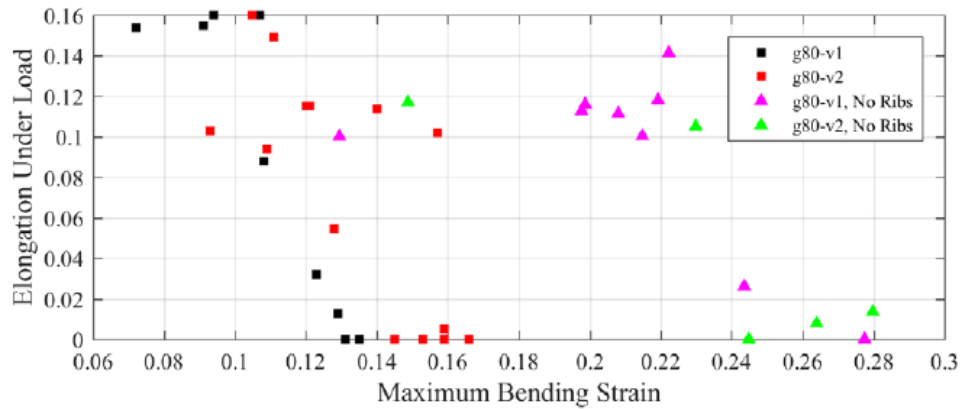


**Figure 3.8** BBT results for rebars with and without ribs [4]

six tests per corrosion level will be sufficient however, more tests will be performed if necessary. The results obtained will be compared to those of a pristine condition rebar which corresponds to a corrosion level of  $CL = 0\%$

**Table 3.2** Corroded Rebar Test Matrix

Corroded rebar test matrix			
Test	Diameter of bar	CL (%)	Number of Tests
Tension test	#6	0	3
		5	3
		10	3
		15	3
		20	3
		25	3
BBT test	#6	0	6
		5	6
		10	6
		15	6
		20	6
		25	6

### **3.2 Expected outcomes from experimental phase**

The results from the tension tests will help to establish if the depassivation process in the corroded rebars has an effect on the measured stress-strain relationship of steel as has been observed in previous research which did not consider the depassivation process [35],[61],[11]. Similarly the results from the BBT tests will show any changes in the critical bending strain of rebars as they corrode. The critical bending strain impacts the bar fracture limit state. In the case of corroded rebars it is expected that the critical bending strain will be modified by changes in the mechanical properties of steel due to corrosion, and effects of concentrated corrosion along the surface of the rebars. These two factors we hypothesize will induce fracture at a lower bending strain than those observed in pristine conditions rebars[5].

The results obtained from the experiment will also be used to define the bar fracture limit state for RC columns. Research currently being developed at NC State will provide models that allow to establish bar fracture tensile strain while considering different parameters such as transverse steel spacing, axial load ratio, strength of the concrete to mention a few. The model will be similar to that presented by Barcley et al [4] shown in EQ. This model could then be implemented in the analytical model presented in 4. If fracture occurs at a lower strain in corroded rebars, this implies that the corroded RC columns are prone to reach the fracture bar limit state at a much lower displacement than in a pristine RC column.

Future studies will verify the application of the results found in this research to perform full scale corroded RC column that consider the effect of depassivation in the cyclic behavior of such columns.

# Chapter 4

## Methodology

A methodology that incorporates the different sources of cumulative damage in RC structures is proposed. Different models of aging conditions that modify the material properties are studied, these are then incorporated into the analytical model.

The aging conditions focused on this research are:

- Corrosion
- Strain aging

Other aging conditions, such as concrete strength aging, repairs, welding and fatigue in steel structures, will be added later to this study.

### 4.1 Modeling of corrosion for structural analysis

Corrosion has been shown to modify the mechanical properties of steel, as discussed in section 2.1. These findings have been incorporated in the structural analysis at the material level. Results obtained from the experimental phase outlined in 3 will be incorporated in this analysis. The incorporation of corrosion in the analytical model is outlined as follows:

1. The time for initiation of corrosion is calculated with equation Eq. 2.2
2. The rate of corrosion is calculated according equation Eq. 2.3
3. The diameter of the rebar is reduced and the corrosion level is calculated using equations Eq. 2.5 Eq. 2.4

- The mechanical properties of the reinforcing steel are modified with the corresponding corrosion level as shown in equation Eq. 2.6

This process is shown in Fig. 4.1.

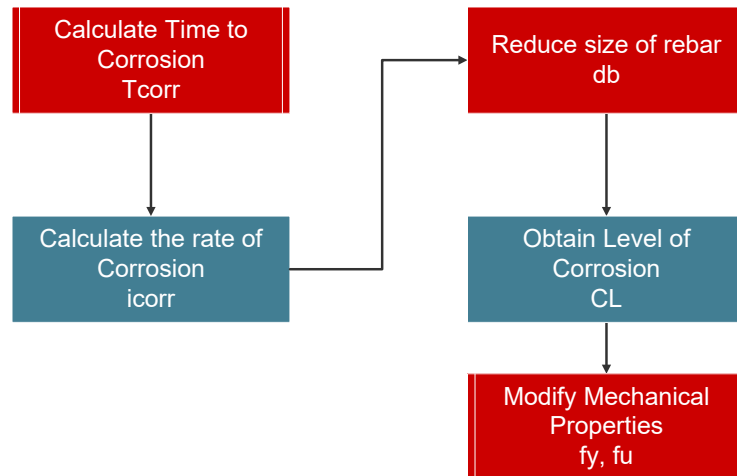


**Figure 4.1** Corrosion modeling for structural analysis

This is later incorporated into the nonlinear structural analysis framework using OpenSeesPy [34][63], the framework of this analysis is explained in section 4.6.

## 4.2 Modeling of strain aging for structural analysis

In mild steel such as grade 60 reinforcing steel the phenomenon of strain aging is of importance. Summarizing the strain aging process described in section 2.2, mild steel after being subjected to high strain, and after time has passed, the yield strength of the steel increases and the fracture strain decreases. The increase in strength of steel is

## 4.3 Multiple seismic events

The evaluation of multiple seismic events is a topic that has been scarcely studied, however their effects have been felt in numerous earthquake sequences such as the Christchurch 2010,

Umbria-Marche Earthquake 1997 and the Puerto Rico Earthquakes 2020. The hypothesis is that accumulation of damage will restart in a smaller seismic event to achieve a prescribed limit state, similar to how corrosion and other aging phenomena might impact the intensity needed to achieve a future limit state.

For this study it has been determined that not all damage in structures are dependent on multiple events but rather their condition when an event occurs as is the case for corrosion. Other damage related phenomena such as strain aging depend on the loading history and are therefore dependent on the history of extreme loading events. It is therefore proposed to study corrosion on a discrete modeling of main shocks each independent of the other and to study the effect on strain aging by using a sequence of Main Shocks.

#### 4.3.1 Earthquake selection

For this study the NGA2 West Database of earthquake records provided by the Pacific Earthquake and Engineering Research Institute (PEER) [2] is used. This database consists of 599 different earthquake events that characterize the ground motions on the west coast of the contiguous United States. The data was filtered according to the following criteria:

- Must be an earthquake sequence
- Moment magnitude  $M_w \geq 5$
- $PGA > 0.04$
- $PGV > 1 \text{ cm/s}$
- $V_{s30} > 100 \text{ m/s} \& V_{s30} < 1000 \text{ m/s}$
- Lowest usable frequency is less than 1Hz
- $R_{rup} < 60 \text{ km}$

From this data the main shocks found are the following earthquakes which can be summarized in Fig. 4.2. Figure 4.2 shows the earthquakes as moment magnitude Mw vs rupture distance ( $R_{rup}$ ).

- Chi-chi
- Managua

- Livermore
- Northridge
- Duzce
- Mammoth lake

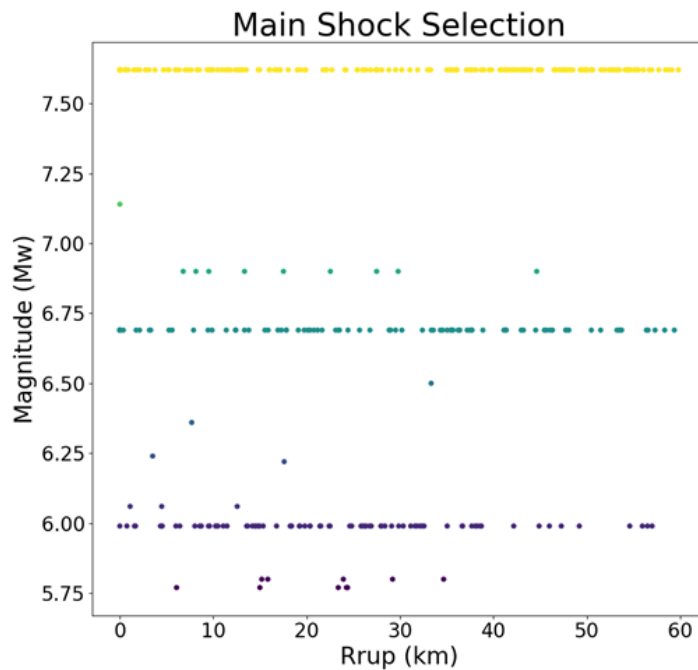


**Figure 4.2** Mainshock selection from PEER NGA West2 database

#### 4.3.2 Discrete modeling of main shock series

The discrete modeling of mainshocks consists of using individual earthquakes that occur at different times throughout the life of the structures which correlate to a corrosion level (CL), this can be done for each of the main shocks selected after which the following data is obtained and later analyzed:

- Maximum axial strain in confined concrete, cover and reinforcing steel Strains

- Obtain the probability of exceeding a given limit state  $P(\varepsilon > \varepsilon_{LS}, IM)$
- The earthquakes are characterized according to an intensity measure

### 4.3.3 Multiple main shock series

To simulate the life of a structure a mainshock series consisting of 3 mainshocks for a the life of a structure is considered, three phases are considered:

1. At time  $t = 0$  the structure has pristine conditions
2. Mainshock 1: pristine conditions are present. No changes to the material properties is present and no accumulation of damage has occurred.
3. Mainshock 2: significant time after time to corrosion, mainshock 2 occurs and material properties have changed due to corrosion
4. Mainshock 3: corrosion and strain aging have occurred and further modified the properties of the materials.

Similar to the discrete modeling of main shock series the following results can be obtained:

- Maximum axial strain in confined concrete, cover and reinforcing steel Strains
- Obtain the probability of exceeding a given limit state  $P(\varepsilon > \varepsilon_{LS}, IM)$
- The earthquakes are characterized according to an intensity measure

## 4.4 Analytical Model

### 4.4.1 Cantilever column

This study focuses on the behavior of a single degree of freedom (SDOF) system representing a cantilever reinforced concrete column. The column is modeled as shown in Fig. 4.3 This structure is modeled in OpenSeesPy [34][63] using the *forceBeamColumn* element [47]. The forceBeamColumn element is used with two-point Gauss-Radau integration applied in the hinge regions and two-point Gauss integration applied on the element interior for a total of six integration points [47]. The force-based formulation requires only a single element to accurately represent the full nonlinear deformation of the member and the integration scheme selected prevents the loss of objectivity during softening response while also providing integration points at

the member ends [8],[47]. The element requires the length of plasticity be defined at each end of the member, for which the tension-based rectangular plastic hinge length is calculated using the following expressions [21]:

$$L_{pc} = k * L_{eff} + 0.4D \quad (4.1)$$

$$k = 0.2 * (Fu/Fy - 1) \leq 0.08 \quad (4.2)$$

$$L_{pt} = L_{pc} + \gamma * D \quad (4.3)$$

For single bending the parameter  $\gamma$  is:

$$\gamma = 0.33 \quad (4.4)$$

The two-point Gauss-Radau integration is applied such that each end node integration is weighted equal to the specified plastic hinge length, as illustrated in Fig. 4.4. Therefore, strains recorded at the end sections represent accurate values even in the case where deformation localizes to the ends from strain-softening behavior. For the case of the cantilever column considered, only one plastic hinge length is defined, and the opposite end is given an arbitrary unit length.

The section of the column is shown in Fig. 4.5, the section is discretized with concrete and steel material fibers. Concrete fibers are modeled using the *Concrete01* material, modified for confined material strength based on the Mander confined concrete model [33]. The *Steel02* material, based on the Giuffre-Menegotto-Pinto model [15] is used for the longitudinal reinforcement with recommended parameters ( $b = 0.01$ ,  $R0 = 20$ ,  $cR1 = 0.925$ ,  $cR2 = 0.15$ ).

#### 4.4.2 Strain penetration

The strain penetration considers the additional deformation due to anchorage of the reinforcement into the foundation, since tension strain in the reinforcement will drop to zero at a depth equal to the true development length of the rebar [43]. Experimental studies have generally reported that this end rotation contributes up to 35% to the lateral deformation of flexural members[62] and it is, therefore, important to incorporate into the analytical model. A way to capture this effect is by using a zero-length section element implemented in the nonlinear fiber-based analysis of concrete structures, this is available in the material library of OpenSeesPy as *BondSP1* [62] this is the material model used for the steel fibers of the zero-length section element.

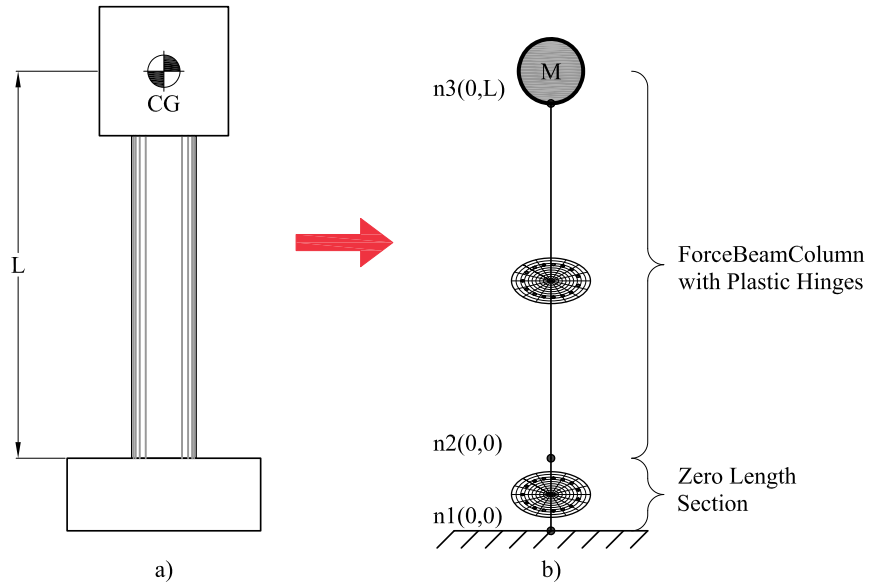


**Figure 4.3** Structural Model a) SDOF Column b) Structural Model

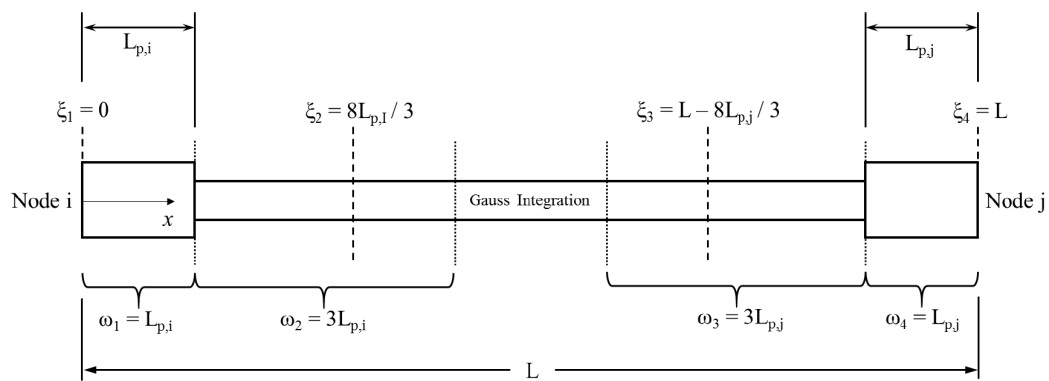


**Figure 4.4** End point plastic hinge method [47]

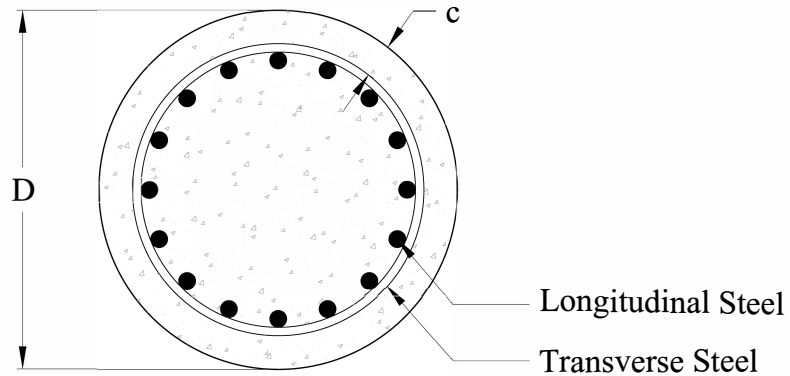


**Figure 4.5** Section of the RC Column

The required parameters for this model are:

- $F_y$  Yield strength of the reinforcement steel
- $S_y$  Rebar slip at member interface under yield stress (see Eq. 4.5)
- $F_u$  Ultimate strength of the reinforcement steel
- $S_u$  Rebar slip at the loaded end at the bar fracture strength a value of  $35S_y$  is recommended [62]
- $b$  Initial hardening ratio in the monotonic slip vs. bar stress response  $b = 0.45$  is recommended [62]
- $R$  Pinching factor for the cyclic slip vs. bar response  $R = 1.01$  is recommended [62]
- $d_b$  Rebar diameter
- $f'c$  Concrete compressive strength of the adjoining connection member
- $\alpha$  Parameter used in the local bond-slip relation and can be taken as  $\alpha = 0.4$  in accordance with CEB-FIP Model Code 90 [10]

Bar slip is calculated as:

$$S_y(\text{in}) = 0.1 \left( \frac{d_b F_y}{4000 \sqrt{f'_c}} (2\alpha + 1) \right)^{\frac{1}{\alpha}} + 0.013(\text{in}) \quad (4.5)$$

#### 4.4.3 Design limit states

Design limit states are defined based on strains in the material since they can more accurately represent the different performance levels of a structure. Structure limit states are defined for tension strains in the rebars or compression strains in the concrete core. The values recommended in typical performance-based design of reinforced concrete bridge columns are shown in Table 4.1. The serviceability limit states correspond to the compression strain at which concrete cover begins to crush and the peak tension strain which results in residual crack widths of approximately 1 mm. These limits are generally accepted as nominal limit states for RC members. The compression limit state for damage control is defined by the expression shown in eq. 4.6 and it refers to the compression strain in the confined concrete at which fracture of the transverse reinforcement confining the core occurs [43]. This equation is obtained using the strain-energy balance between that absorbed by the confined core concrete and the capacity of the confining steel. The tension damage control limit state is defined by the strain at the onset of buckling which can be expressed according to 4.7, this equation demonstrated accurate predictions of the onset of bar buckling on physical tests in SDOF Concrete Column [20]. The bar buckling limit state could change as a result of the experimental campaign proposed in Chapter 4.

$$\varepsilon_{c,spiralyield} = 0.009 - 0.3 \frac{A_{st}}{A_g} + 3.9 \frac{f_{yhe}}{E_s} \quad (4.6)$$

$$\varepsilon_{s,BB} = 0.03 + 700\rho_s \frac{f_{yhe}}{E_s} - 0.1 \frac{P}{f'_c A_g} \quad (4.7)$$

**Table 4.1** Design limit states

Limit State	Concrete Limit State $\varepsilon_c$ (in/in)	Reinforcing Steel Limit State $\varepsilon_s$ (in/in)
Serviciability	0.004	0.015
Damage Control	Eq. 4.6	Eq. 4.7

## 4.5 Comparison with existing physical tests

### 4.5.1 Pristine condition columns

Goodnight et al performed a total of 30 circular RC columns quasi-static tests to evaluate strain limit states [20]. From this set of tests, a sample of one was taken to calibrate the analytical model. The test performed by Goodnight et al on an SDOF cantilever column shows similar geometry to that presented in Fig. 4.4. The parameters used in this large scale test were:

- Diameter  $D = 24.0\text{inch}$
- Height of the column  $L = 8.0\text{ft}$
- Yield strength of steel  $f_y = 574.0\text{MPa}$
- Ultimate strength of steel  $f_u = 753.3 * \text{MPa}$
- Longitudinal steel volumetric ratio  $\rho_s = 1.5\%$
- Transverse steel volumetric ratio  $\rho_v = 1.0\%$
- Strength of concrete at 8 days  $f'_c = 39.8\text{MPa}$

The analytical model utilized these parameters to compare the results from the model to the experimental results. The results from the analysis show good agreement with the experimental results as evidenced in Fig. 4.6. This assures that the results obtained from the model predict the overall system behavior and can be used to analyze other configurations of the structural model.

### 4.5.2 Accelerated corrosion columns

Similarly, Ma et al performed a series of quasi-static tests on RC columns with different corrosion levels and axial load ratios [29]. From their study, the test with a corrosion level  $CL = 9.5\%$  was taken for calibration since the other tests presented in their study had excessively high axial load ratios which are not common in RC bridges. The results from Ma et al test [29] were used to compare against the analytical model. The column had the following parameters:

- Diameter  $D = 260.0\text{mm}$
- Height of the column  $L = 820.0\text{mm}$

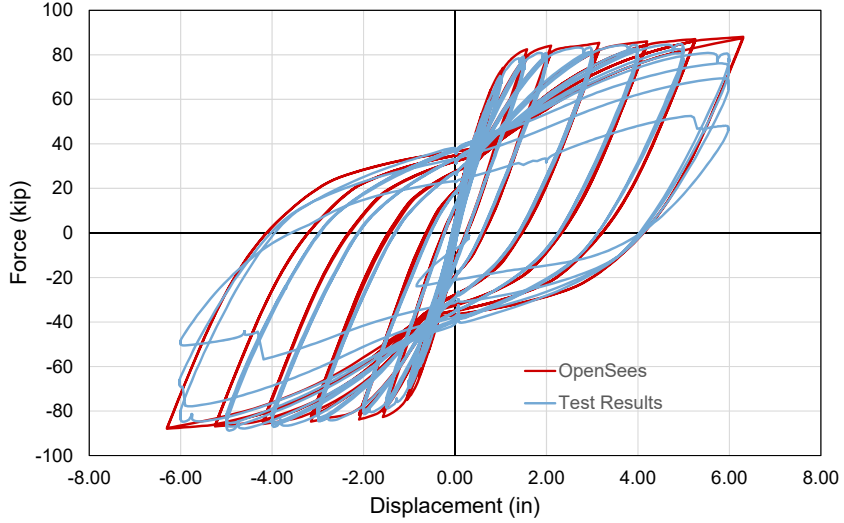


**Figure 4.6** Force-Displacement results from experimental results [21] and analytical model

- Yield strength of steel  $f_y = 375.0$  MPa
- Ultimate strength of steel  $f_u = 572.3$  MPa
- Longitudinal steel volumetric ratio  $\rho_s = 1.5\%$
- Transverse steel volumetric ratio  $\rho_v = 1.0\%$
- Strength of concrete at 8 days  $f'_c = 39.8$  MPa
- Corrosion level  $CL = 9.5\%$

In the analysis equation Eq. 2.6 is used to modify the material properties of the reinforcing steel, to consider the effects of corrosion. Figure 4.7 shows that the results obtained from the analytical model capture the response of the structure with some accuracy. Ma et al [29] did not report if bar buckling and bar fracture occurred during the test. However, the hysteresis curve shown in their study suggests that some damage limit state was reached. To corroborate this, equation Eq. 4.7 is used to determine the bar buckling limit state ( $\varepsilon_{s,BB} = 0.024$ ), this is then compared to the analytical model results shown in figure Fig. 4.8. The results show a peak tension strain of  $\varepsilon_s = 0.023$ . This result is close to the value obtained using equation Eq. 4.7, thus pointing out the likelihood that the bar buckling limit state was observed during this test. While these results are close, it is still not clear if equation Eq. 4.7 captures the behavior of the

buckling limit state for corroded rebars, therefore, the proposed corroded BBT test will show if corrosion affects the behavior of buckled bars.

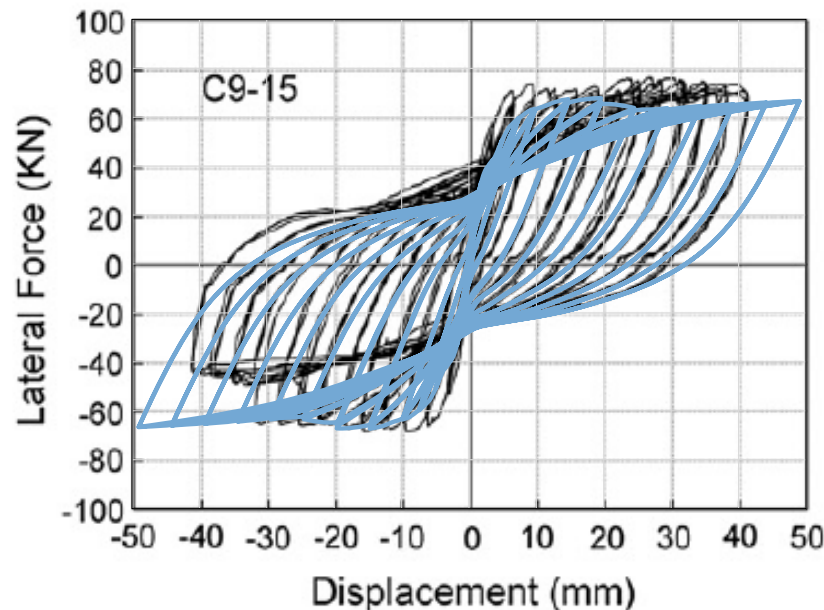


**Figure 4.7** Force-Displacement results from experimental RC column with corrosion in longitudinal bar (CL=9.5%) results [29] and analytical model (shown in lightblue)

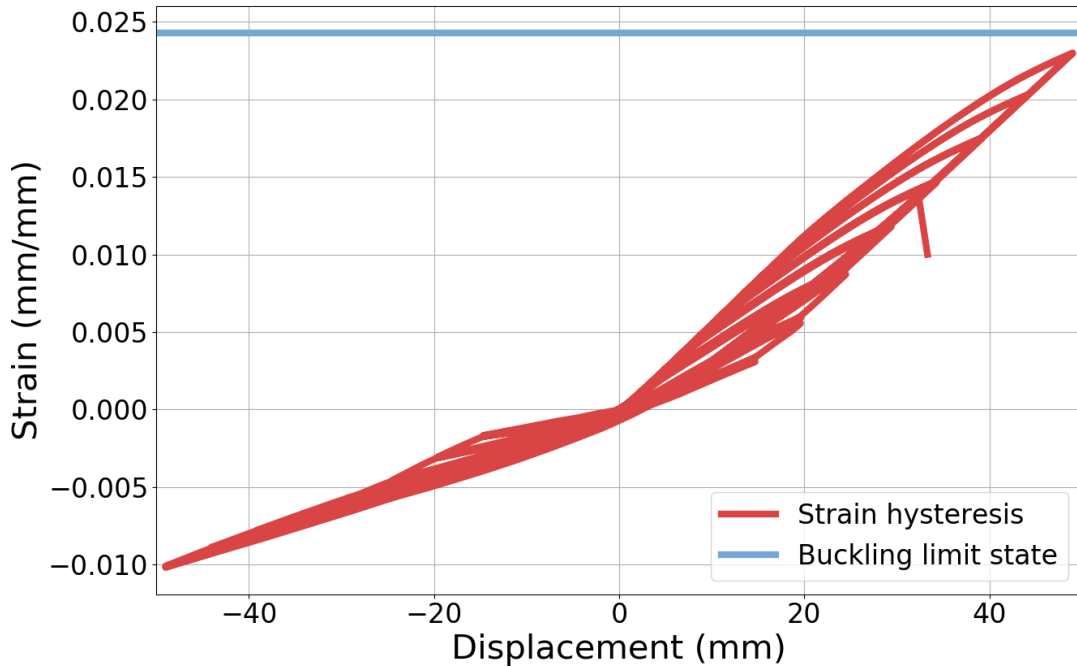


**Figure 4.8** Strain hysteresis from experimental RC column with corrosion in longitudinal bar (CL=9.5%) results from analytical model

## 4.6 Analytical framework

An analytical framework is established to obtain the change in the structure performance due to aging conditions and evaluate the effect of multiple seismic events. Therefore, a series of nonlinear time history analyses (NLTHA) will be performed. From these analyses, it is possible to determine the effects of damage in the performance of structures. The proposed analytical framework process consists of:

1. Geometrical properties of the SDOF column
2. Properties of the material are evaluated (i.e. water to cement ratio, cover)
3. For equal periods of time the time dependent properties are modified
4. Nonlinear time history analyses are performed for discrete ground motions or sequence of ground motions
5. Results are obtained and evaluated

The analysis matrix for the corrosion aging phenomenon that will be analyzed in this study is shown in Table 4.2. The area or extent covered in the analysis corresponds to the range of variables that are common for RC columns in bridges.

**Table 4.2** Analysis matrix

ANALYSIS MATRIX		
Description	Parameter	Range
Diameter of Column	D	30-90 in
Column Length to Diameter Ratio	L/D	2-8
Longitudinal Ratio	$\rho_s$	0.01-0.04
Transverse Volumetric Ratio	$\rho_v$	0.005-0.015
Axial Load Ratio	ALR	0.05-0.2
water to cement ratio	w/c	0.36-0.6
cover	c	1.5-3 in
Time/Condition	CL	5%-20%

## 4.7 Results from NLTHA

This section presents the results obtained from a non-linear time history analysis (NLTHA) performed using OpenSeesPy [63]. The structure was subjected to a total of 18 earthquake records. The main responses obtained from these analyses correspond to the maximum strain obtained for the different levels of corrosion.

The structure used for this results currently corresponds to the parameters shown in section 5.2.1. The structure was analyzed for a range of corrosion levels [1.5%-13%] in the longitudinal rebars.

### 4.7.1 Effect on structure response

An example of the results obtained using NLTHA, figures Fig. 4.9 and Fig. 4.10 are presented. These results are extracted from the response of the structure to the Chi-Chi earthquake. Fig. 4.9 shows the global system response and Fig. 4.10 shows the stress-strain response of the extreme fiber of reinforcing steel. These results show that as corrosion increases the demands imposed on the structure increases too. Therefore an increase in the probability of reaching a limit state increases as corrosion increases.

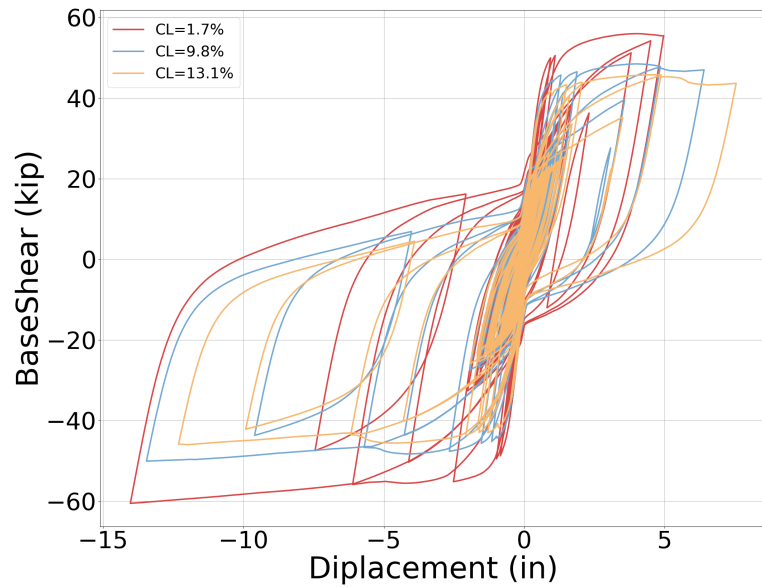


**Figure 4.9** Force-Displacement results

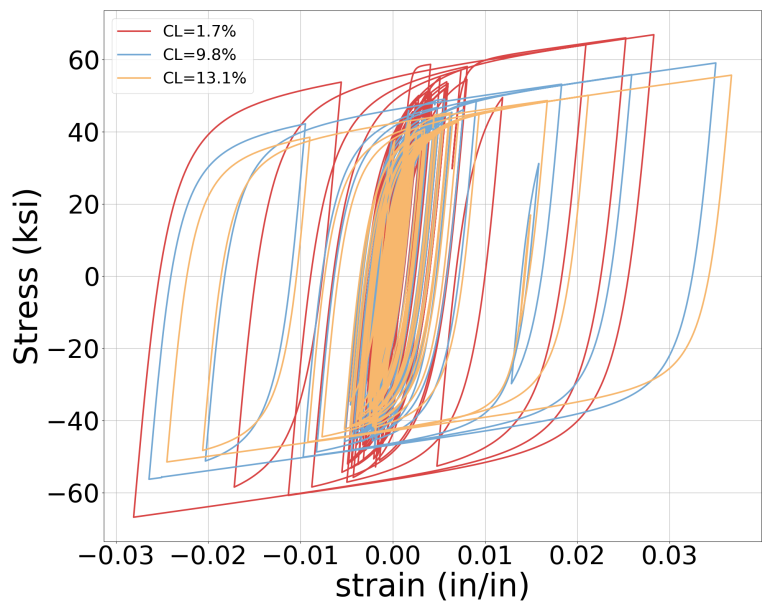


**Figure 4.10** Stress strain response for extreme rebar location

#### 4.7.2 Development of cumulative distribution functions

Once the analysis is complete the data is post-processed and expressed as a cumulative distribution function (CDF). The methodology employed corresponds to the multiple stripe analysis (MSA) recommended by Baker et al [3]. While peak ground acceleration ( $PGA$ ) has been widely used as the intensity measure to develop fragility functions[19][6][49], Krish [27] in a recent study, showed that spectral displacement at first effective period ( $IM = Sd(T_1)$ ) has better correlation than  $PGA$ . To demonstrate this, CDF curves were developed for  $IM = PGA$  and  $IM = Sd(T_1)$ , and are shown in figures Fig. 4.11 and Fig. 4.12 correspondingly. The CDFs were developed for the steel yielding limit state, however this can be extrapolated for any limit state. Fig. 4.11 shows the results obtained with  $IM = PGA$  do not show a good correlation since as corrosion increases the probability of exceeding a limit state decreases, this is not the behavior observed in Fig. 4.10. Conversely, Fig. 4.12 shows the results with  $IM = Sd(T_1)$ , these results present a better correlation, since, as corrosion increases, the probability of exceeding the limit state of yielding increases, for the preliminary results shown here the corrosion level of 13.1% results are an exception. These results will improve as more analyses become available.

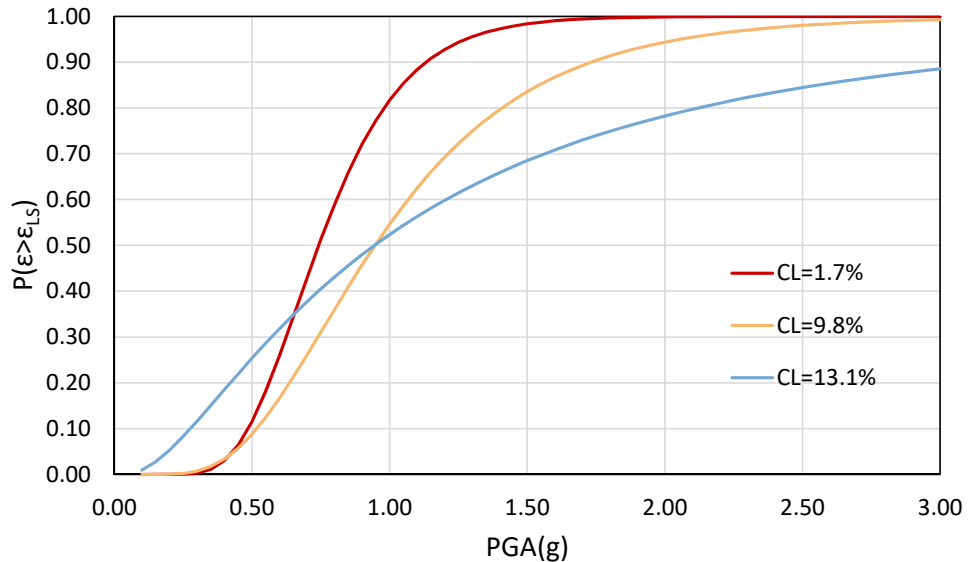


**Figure 4.11** CDF of steel yielding limit state using  $IM = PGA$

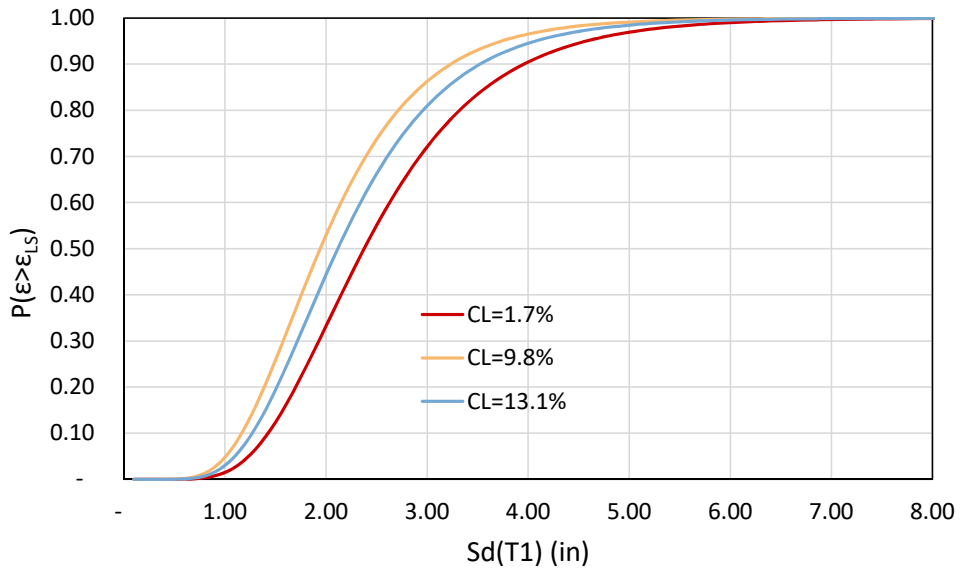


**Figure 4.12** CDF of steel yielding limit state using  $IM = Sd(T_1)$

#### 4.7.3 Results discussion

- The results show that there is an increase in the demands as the corrosion in the structure increases. This is clearly shown in Fig. 4.12. However, more results will help improve this correlation
- Results shown in Fig. 4.11 and Fig. 4.12, show that  $IM = Sd(T_1)$  is a better intensity measure than  $IM = PGA$
- The outcomes from the experimental campaign will further improve the results obtained in the analytical work
- The experimental phase will also provide an improved methodology to mimic the behavior of corroded reinforcing steel that is embedded inside the concrete
- The inclusion of additional aging conditions in the analysis will provide a realistic analysis of aging RC columns

#### 4.8 Future topics

- Concrete strength aging

- Welding and fatigue in steel structures
- Repair effects
- Main shock - after shock series - repair series
- Load history effects
- Degree of damage effect on confined structures behavior
- Selection of intensity measure (IM)

## **Chapter 5**

# **Expected findings and schedule of work**

In this chapter first a framework for the analysis that is performed is presented, later the basic model that is used for the analysis is presented and later calibrated and verified with experimental data available in the literature. Finally, preliminary results are presented that will give a first view of the proposed research.

## BIBLIOGRAPHY

- [1] Amato, A., Azzara, R., Chiarabba, C., Cimini, G. B., Cocco, M., Di Bona, M., Margheriti, L., Mazza, S., Mele, F., Selvaggi, G., Basili, A., Boschi, E., Courboulex, F., Deschamps, A., Gaffet, S., Bittarelli, G., Chiaraluce, L., Piccinini, D. & Ripepe, M., "The 1997 Umbria-Marche, Italy, earthquake sequence: A first look at the main shocks and aftershocks," *Geophysical Research Letters*, **25**, no. 15, pp. 2861–2864, 1998.
- [2] Ancheta, T. D., Darragh, R. B., Stewart, J. P., Seyhan, E., Silva, W. J., S-J Chiou, B., Wooddell, K. E., Graves, R. W., Kottke, A. R., Boore, D. M., Kishida, T. & Donahue, J. L., "NGA-West2 Database," 2014.
- [3] Baker, J. W., "Efficient analytical fragility function fitting using dynamic structural analysis," *Earthquake Spectra*, **31**, no. 1, pp. 579–599, 2015.
- [4] Barcley, L., "Seismic Performance of A706-80 Reinforced Concrete Columns and Critical Bending Strain of Longitudinal Reinforcement," PhD thesis, North Carolina State University, 2018.
- [5] Barcley, L. & Kowalsky, M., "Critical Bending Strain of Reinforcing Steel and Buckled Bar Tension Test," *ACI Materials Journal*, **116**, no. 3, 2019.
- [6] Bisadi, V. & Padgett, J. E., "Explicit time-dependent multi-hazard cost analysis based on parameterized demand models for the optimum design of bridge structures," *Computer-Aided Civil and Infrastructure Engineering*, **30**, no. 7, pp. 541–554, 2015.
- [7] Bradley, B. A. & Cubrinovski, M., "NEAR-SOURCE STRONG GROUND MOTIONS OBSERVED IN THE 22 FEBRUARY 2011 CHRISTCHURCH EARTHQUAKE," Tech. Rep.
- [8] Calabrese, A., Almeida, J. P. & Pinho, R., "Numerical issues in distributed inelasticity modeling of rc frame elements for seismic analysis," *Journal of Earthquake Engineering*, **14**, no. sup1, pp. 38–68, 2010.
- [9] Choe, D.-E., Gardoni, P., Rosowsky, D. & Haukaas, T., "Probabilistic capacity models and seismic fragility estimates for RC columns subject to corrosion," *Reliability Engineering & System Safety*, **93**, no. 3, pp. 383–393, 2008.
- [10] Comité Euro-Intenational du Betón, *CEB-FIP Model Code 90*, 1st. London, 1993.
- [11] Du, Y. G., Clark, L. A. & Chan, A. H. C., "Residual Capcaity of Corroded Reinforcing Bars," *Magazine of Concrete Research*, **57**, no. 3, pp. 135–147, 2005.
- [12] Enright, M. P. & Frangopol, D. M., "Probabilistic analysis of resistance degradation of reinforced concrete bridge beams under corrosion," *Engineering Structures*, **20**, no. 11, pp. 960–971, 1998.

- [13] Fajfar, P., “Equivalent ductility factors, taking into account low-cycle fatigue,” *Earthquake Engineering & Structural Dynamics*, **21**, no. 10, pp. 837–848, 1992.
- [14] FEMA, “Prestandard and Commentary for the Seismic Rehabilitation of Buildings,” *Rehabilitation Requirements*, no. 1, pp. 1–518, 2000.
- [15] Filippou, F. C., Popov, E. & Bertero, V., “Effects of bond deterioration on hysteretic behavior of reinforce concrete coint,” Tech. Rep. August, 1983, p. 212.
- [16] Ghods, P., Isgor, O. B., McRae, G. & Miller, T., “The effect of concrete pore solution composition on the quality of passive oxide films on black steel reinforcement,” *Cement and Concrete Composites*, **31**, no. 1, pp. 2–11, 2009.
- [17] Ghods, P., Isgor, O. B., McRae, G. A. & Gu, G. P., “Electrochemical investigation of chloride-induced depassivation of black steel rebar under simulated service conditions,” *Corrosion Science*, **52**, no. 5, pp. 1649–1659, 2010.
- [18] Ghosh, J. & Padgett, J. E., “Aging Considerations in the Development of Time-Dependent Seismic Fragility Curves,” *Journal of Structural Engineering*, **136**, no. 12, pp. 1497–1511, 2010.
- [19] Ghosh, J., Padgett, J. E. & Sánchez-Silva, M., “Seismic Damage Accumulation in Highway Bridges in Earthquake-Prone Regions,” *Earthquake Spectra*, **31**, no. 1, pp. 115–135, 2015.
- [20] Goodnight, J. C., Kowalsky, M. J. & Nau, J., “Strain limit states for circular rc bridge columns,” *Earthquake Spectra*, **32**, no. 3, pp. 1627–1652, 2016.
- [21] Goodnight, J. C., Kowalsky, M. J. & Nau, J. M., “Effect of load history on performance limit states of circular bridge columns,” *Journal of Bridge Engineering*, **18**, no. 12, pp. 1383–1396, 2013.
- [22] Hatzigeorgiou, G. D. & Beskos, D. E., “Inelastic displacement ratios for SDOF structures subjected to repeated earthquakes,” *Engineering Structures*, **31**, pp. 2744–2755, 2009.
- [23] Hosseini, S., Heidarpour, A., Collins, F. & Hutchinson, C. R., “Effect of strain ageing on the mechanical properties of partially damaged structural mild steel,” *Construction and Building Materials*, **77**, pp. 83–93, 2015.
- [24] Jensen, O. M., Hansen, P. F., Coats, A. M. & Glasser, F. P., “Chloride ingress in cement paste and mortar,” *Cement and Concrete Research*, **29**, no. 9, pp. 1497–1504, 1999.
- [25] Khashaee, P. & Eeri, M, “Damage-based Seismic Design of Structures,” *Earthquake Spectra*, **21**, no. 2, pp. 371–387, 2005.

- [26] Krawinkler, H., “Performance Assessment of Steel Component,” *Earthquake Spectra*, **3**, no. 1, pp. 27–41, 1987.
- [27] Krish, Z. F., “Rapid Repair of Reinforced Concrete Bridge Columns Subjected to Seismic Loading via Plastic Hinge Relocation,” PhD thesis, North Carolina State University, 2018.
- [28] Kunnath, S. K., Reinhorn, A. M. & Lobo, R. F., “IDARC Version 3.0: A Program for the Inelastic Damage Analysis of RC Structures,” **818**, no. 1992, pp. 1–20, 1992.
- [29] Ma, Y., Che, Y. & Gong, J., “Behavior of corrosion damaged circular reinforced concrete columns under cyclic loading,” *Construction and Building Materials*, **29**, pp. 548–556, 2012.
- [30] Mackie, K. R. & Stojadinović, B., “Performance-based seismic bridge design for damage and loss limit states,” *Earthquake Engineering & Structural Dynamics*, **36**, no. 13, pp. 1953–1971, 2007.
- [31] Mackie, K. R. & Stojadinović, B., “Seismic demands for performance based design of bridges,” *Pacific Earthquake Engineering Research Center, PEER Repor*, no. August, p. 156, 2003.
- [32] Manafpour, A. R. & Kamrani Moghaddam, P., “Performance capacity of damaged RC SDOF systems under multiple far- and near-field earthquakes,” *Soil Dynamics and Earthquake Engineering*, **116**, pp. 164–173, 2019.
- [33] Mander, J. B., Priestley, M. J. N. & Park, R., “Theoretical stress-strain model for confined concrete,” *Journal of Structural Engineering*, **114**, no. 8, pp. 1804–1826, 1988.
- [34] McKenna, F., Scott, M. H. & Fenves, G. L., “Nonlinear finite-element analysis software architecture using object composition,” *Journal of Computing in Civil Engineering*, **24**, no. 1, pp. 95–107, 2010.
- [35] Meda, A., Mostosi, S., Rinaldi, Z. & Riva, P., “Experimental evaluation of the corrosion influence on the cyclic behaviour of RC columns,” *Engineering Structures*, **76**, pp. 112–123, 2014.
- [36] Mehta, P. K. & Monteiro, P. J. M., *Concrete: Microstructure, Properties, and Materials*, 4th ed. McGraw Hill, 2014.
- [37] Miranda, E., Archbold, J., Heresi, P., Messina, A., Rosa, I., Robertson, I., Mosalam, K., Kijewski-Correa, T., Prevatt, D. & Roueche, D., “PRJ-2712 — StEER - Puerto Rico Earthquake Sequence December 2019 to January 2020: Field Assessment Structural Team (FAST) Early Access Reconnaissance Report (EARR),” Structural Extreme Events Reconnaissance, Tech. Rep., 2020, p. 173.

- [38] Momtahan, A., Dhakal, R. P. & Rieder, A., “Effects of strain-ageing on New Zealand reinforcing steel bars,” *Bulletin of the New Zealand Society for Earthquake Engineering*, **42**, no. 3, pp. 179–186, 2009.
- [39] NIED K-NET KiK-net, *K-NET, KiK-net*, 2019.
- [40] Northern Digital Inc., *OPTOTRAK Certus HD dynamic measuring machine*, 2020.
- [41] Overby, D., Kowalsky, M. & Seracino, R., “Stress-strain response of A706 grade 80 reinforcing steel,” *Construction and Building Materials*, **145**, pp. 292–302, 2017.
- [42] Padgett, J. E. & Desroches, R., “Bridge Functionality Relationships for Improved Seismic Risk Assessment of Transportation Networks,” *Earthquake Spectra*, **23**, no. 1, pp. 115–130, 2007.
- [43] Priestley, M., Calvi, G. M. & Kowalsky, M. J., *Displacement-Based Seismic Design of Structures*, 1st. Pavia, Italy: IUSS Press, 2007.
- [44] Raghunandan, M., Liel, A. B. & Luco, N., “Aftershock collapse vulnerability assessment of reinforced concrete frame structures,” *Earthquake Engineering & Structural Dynamics*, **44**, no. 3, pp. 419–439, 2015.
- [45] Restrepo-Posada, J., Dodd, L. L., Park, R & Cooke, N, “Variables Affecting Cyclic Behavior of Reinforcing Steel,” *Journal of Structural Engineering*, **120**, no. 11, pp. 3178–3196, 1994.
- [46] Roufaiel, M. S. L. & Meyer, C., “Analytical modeling of hysteretic behavior of r/c frames,” Tech. Rep.
- [47] Scott, M. H. & Fenves, G. L., “Plastic Hinge Integration Methods for Force-Based Beam-Column Elements,” *Journal of Structural Engineering*, **132**, no. 2, pp. 244–252, 2006.
- [48] Shearer, P. M., *Introduction to seismillogy*, 2nd editio. Cambridge: Cambridge University Press, 2009, pp. 301–320.
- [49] Shekhar, S., Ghosh, J. & Padgett, J. E., “Seismic life-cycle cost analysis of ageing highway bridges under chloride exposure conditions: modelling and recommendations,” *Structure and Infrastructure Engineering*, **14**, no. 7, pp. 941–966, 2018.
- [50] Stewart, M. G. & Rosowsky, D. V., “Time-dependent reliability of deteriorating reinforced concrete bridge decks,” *Structural Safety*, **20**, no. 1, pp. 91–109, 1998.
- [51] Sunasaka, Y. & Kiremidjian, A. S., “A method for structural safety evaluation under mainshock-aftershock earthquake sequences,” Stanford University, Tech. Rep., 1993.

- [52] Tesfamariam, S., Goda, K. & Mondal, G., “Seismic Vulnerability of Reinforced Concrete Frame with Unreinforced Masonry Infill Due to Main Shock-Aftershock Earthquake Sequences,” *Earthquake Spectra*, **31**, no. 3, pp. 1427–1449, 2015.
- [53] Thoft-Christensen, P., “Corrosion and Cracking of Reinforced Concrete,” *Life-Cycle Performance of Deteriorating Structures: Assessment, Design and Management*, 2003, pp. 26–36.
- [54] Vamvatsikos, D. & Allin Cornell, C., “Incremental dynamic analysis,” *Earthquake Engineering and Structural Dynamics*, **31**, no. 3, pp. 491–514, 2002.
- [55] Vu, K. A. T. & Stewart, M. G., “Structural reliability of concrete bridges including improved chloride-induced corrosion models,” *Structural Safety*, **22**, no. 4, pp. 313–333, 2000.
- [56] Weyers, R. E., Fitch, M. G., Larsen, E. P., Al-Qadi, I. L., Chamberlin Albany, W. P., York, N. & Hoffman, P. C., “Service Life Estimates,” Strategic Highway Research Program, Washington DC, Tech. Rep., 1994.
- [57] Williams, M. S. & Sexsmith, R. G., “Seismic Damage Indices for Concrete Structures: A State-of-the-Art Review,” *Earthquake Spectra*, **11**, no. 02, pp. 319–349, 1995.
- [58] Y. Liu & R. E. Weyers, “Modeling the Time to Corrosion Cracking in Chloride contaminated Reinforced Concrete Structures,” *ACI Materials Journal*, **95**, no. 6, pp. 675–680, 1998.
- [59] Yang, S.-Y., Song, X.-B., Jia, H.-X., Chen, X. & Liu, X.-L., “Experimental research on hysteretic behaviors of corroded reinforced concrete columns with different maximum amounts of corrosion of rebar,” *Construction and Building Materials*, **121**, pp. 319–327, 2016.
- [60] Young-Ji Park, B., H-S Ang, A. & Asce, F., “Mechanistic seismic damage model for reinforced concrete,” *Journal of Structural Engineering*, **111**, no. 4, pp. 722–739, 1985.
- [61] Yuan, Z., Fang, C., Parsaeimaram, M. & Yang, S., “Cyclic Behavior of Corroded Reinforced Concrete Bridge Piers,” *Journal of Bridge Engineering*, **22**, no. 7, 2017.
- [62] Zhao, J. & Sritharan, S., “Modeling of strain penetration effects in fiber-based analysis of reinforced concrete structures,” *ACI Structural Journal*, **104**, no. 2, pp. 133–141, 2007. arXiv: [arXiv:1011.1669v3](https://arxiv.org/abs/1011.1669v3).
- [63] Zhu, M., McKenna, F. & Scott, M. H., “OpenSeesPy: Python library for the OpenSees finite element framework,” *SoftwareX*, **7**, pp. 6–11, 2018.